THE EFFECTS OF HURRICANE HARVEY ON METHYL HALIDE SOURCES AND SINKS IN GALVESTON BAY, TX AND THE WEST TEXAS SHELF

A Thesis

by

DAMIAN SCOTT SIMONINI

Submitted to the Office of Graduate and Professional Studies of
Texas A&M University
in partial fulfillment of the requirements for the degree of

MASTER OF SCIENCE

Chair of Committee,	Shari Yvon-Lewis
Co-Chair of Committee,	Daniel C.O. Thornton
Committee Members,	Peter Santschi
	Yina Liu
Head of Department,	Shari Yvon-Lewis

August 2018

Major Subject: Oceanography

ABSTRACT

Methyl halides, methyl chloride (CH_3Cl), methyl bromide (CH_3Br), and methyl iodide (CH_3I), play an important role in atmospheric chemistry, because they deplete ozone through catalytic ozone destruction. Measurements of CH_3Cl, CH_3Br, and CH_3I were made at a combination of 14 different sampling locations in Galveston Bay during four sampling periods: June, September, November of 2017, and March of 2018. The September measurements were made after Hurricane Harvey had introduced over 42 billion cubic meters of water to the surrounding area.

Over a one year period the average atmospheric concentrations for CH_3Cl, CH_3Br, and CH_3I were 612.7ppt, 12.60ppt, and 2.35ppt, respectively. In June, CH_3Br and CH_3I concentrations were 64% and 122% above the one year average. This significant elevation in June concentrations were likely linked to methyl halide emissions from rice paddy production in Arkansas. The one year average water concentrations for CH_3Cl, CH_3Br, and CH_3I were 123.1pM, 3.07pM, and 6.99pM respectively. In September, methyl halides concentrations were lower due to a precipitation driven freshwater flushing of the bay. Correlations between the methyl halide concentrations suggest they have a common source in the bay. Highest concentrations of methyl halides were seen in the center of the bay with lowest near the mouth of the Trinity River. Overall, spatial distributions of water concentrations appear to be driven by dilution, freshwater flows into the bay by the Trinity and San Jacinto Rivers and their effects on biological productivity. The one year average sea-to-air flux for CH_3Cl, CH_3Br and CH_3I was 28.2nmol m^{-2} d^{-1}, 0.71nmol m^{-2} d^{-1}, and 3.71nmol m^{-2} d^{-1} respectively.

Along the West Texas Shelf in October 2017, the CH_3Cl, CH_3Br, and CH_3I average water concentrations were 140.7pM, 2.48pM, and 5.63pM and the average sea-to-air fluxes were 173.21nmol m^{-2} d^{-1}, 2.35nmol m^{-2} d^{-1}, 13.51nmol m^{-2} d^{-1} respectively. The higher sea-to-air fluxes along the coast were partially due to overall higher saturation states, but mainly due to higher average wind speeds during the sample period. Including emissions from coastal areas to overall global ocean emission predictions could elevate the global ocean emission source by 12.5% and 4.2% for CH_3Cl and CH_3Br respectively.

ACKNOWLEDGEMENTS

I would like to thank both of my committee co-chairs, Dr. Yvon-Lewis and Dr. Thornton for providing me with the opportunity to complete this research. They have served as great sources of information and support during the completion of my thesis. I would also like to acknowledge my other committee members Dr. Santschi and Dr. Liu for their useful input on my research.

To my wonderful parents, Greg and Tracy Simonini, I would like to thank them for doing everything a parent can do from 1,000 miles away to help me during my time at Texas A&M University. They taught me at a young age that anything is possible with hard work and passion and that has stayed with throughout my life. They also provided financial and emotional support, this allowed me to not have to worry about the little stuff when I had much bigger things at hand. I would also like to extend thanks to the rest of my family for their support: Shane and Zack Simonini as well as Angel, Mike, Dylan, and Payton Campese.

A special thank you goes to my lab partner Stanford Goodwin, for the countless hours him and I spent together building the sample module and working on the GC-MS. He helped me understand the mechanics behind the GC-MS and how to run it. He kept the GC-MS running through all of our sampling even with the frustrations it was giving us. I would also like to thank Laramie Jensen and the other graduate and undergraduate students that made the sampling trips possible.

Thank you to all the friends I have made along the way in both my undergraduate years at Purdue and my graduate years at Texas A&M University. You have helped me unwind from long weeks of work and celebrate when work is well done, maybe a little too often. Without all

of you my time at both universities would not have been as amazing as it was. Thank you for making the last six years of my left unforgettable.

Lastly thank you to the whole Department of Oceanography at Texas A&M University. From the students in my cohort, to Oceanography Graduate Council, to the professors who taught me and that I taught for. You gave me the opportunities to excel at Texas A&M University and supported me along the way.

CONTRIBUTORS AND FUNDING SOURCES

This work was supervised by a thesis committee consisting of co-chairs Professor Shari Yvon- Lewis and Professor Daniel C. O. Thornton and Professor Yina Liu of the Department of Oceanography and Professor Peter Santschi of the Department of Marine Sciences at Texas A&M Galveston. Graduate summer studies were supported by NSF S-STEM Scholarship program. All work for the thesis was completed independently by the student.

NOMENCLATURE

CH_3Cl	Methyl Chloride
CH_3Br	Methyl Bromide
CH_3I	Methyl Iodide
ODS	Ozone Depleting Substances
CFC	Chlorofluorocarbon
HCFC	Hydrochlorofluorocarbon
CCN	Cloud Condensation Nuclei
EPA	Environmental Protection Agency
SAM	S-Adenosyl-L-Methionine
CDOM	Colored Dissolved Organic Matter
GC-MS	Gas Chromatography-Mass Spectrometer
TAMUG	Texas A&M University Galveston
DIC	Dissolved Inorganic Carbon
PAH	Polycyclic Aromatic Halocarbon
DOC	Dissolved Organic Matter
USGS	United States Geological Survey
NOAA	National Oceanic and Atmospheric Administration
HYSPLT	Hybrid Single Particle Lagrangian Integrated Trajectory
NDBC	National Data Buoy Center

TABLE OF CONTENTS

Page

LIST OF FIGURES

Page

LIST OF TABLES

Page

1. INTRODUCTION

Methyl halides play an important role in both tropospheric and stratospheric atmospheric chemistry because they can deplete stratospheric ozone through catalytic ozone destruction [*Carpenter et al.*, 2014]. Methyl halides including methyl chloride (CH_3Cl), methyl bromide (CH_3Br), and methyl iodide (CH_3I) are produced primarily by natural sources, with anthropogenic sources being strictly regulated[*Carpenter et al.*, 2014]. Once emitted to the atmosphere, methyl halides can reach the stratosphere where they are broken down through photolysis and reactions with hydroxyl radicals, releasing halogen atoms [*Carpenter et al.*, 2014]. CH_3I is broken down within days of being in the atmosphere, releasing iodine primarily to the troposphere, while CH_3Cl and CH_3Br have longer lifetimes of 0.9 and 0.8 years allowing them to be significant contributors of chlorine and bromine to the stratosphere [*Carpenter et al.*, 2014].

In the past, most of the attention from the scientific community focused on anthropogenically produced ozone depleting substances (ODS), such as CH_3Br, chlorofluorocarbons (CFCs), hydrochlorofluorocarbons (HCFCs), chlorinated solvents, and halons [*Butler*, 2000; *Carpenter et al.*, 2014; *Montzka et al.*, 2011]. In the 1990's, the introduction of the Montreal Protocol, and its amendments, put in place strict regulations regarding the anthropogenic production of ODS, including CH_3Br and other volatile halogenated methanes [*Carpenter et al.*, 2014; *Montzka et al.*, 2011]. To better understand the impact of anthropogenic emissions of CH_3Br and other ODS as well as their overall global budget, it is important to understand the natural sources of ODS. Currently the global budgets of CH_3Cl and

CH_3Br are imbalanced, known sinks outweigh the known sources, and there is a lack of data from coastal environments [*Carpenter et al.*, 2014; *Hu et al.*, 2013; *Montzka et al.*, 2011].

Coastal environments are subject to intermittent forces on a seasonal timeframe such as freshwater flow, precipitation, tides, and amount of sunlight received. Large scale events such as droughts, floods, and hurricanes can also play an important role in coastal environments. These environments are unique as they are located in close proximity to both anthropogenic and natural factors that could influence methyl halide production. These factors include marine and atmospheric transportation of methyl halides by terrestrial regions such as wetlands and rice paddies as well as direct influence on marine emissions by nutrient inflows from rivers and industry outfalls.

Here, I discuss the results of a survey of the sources and sinks of methyl halides in Galveston Bay, TX in pre- and post-hurricane conditions and a survey on sources and sinks of methyl halides along the West Texas Shelf following Hurricane Harvey. Galveston Bay, TX and the West Texas Shelf were chosen because methyl halide concentrations and emissions can be high in coastal areas; however, bay environments have not been researched. This study gives us an opportunity to understand how unique environments such as Galveston Bay can affect overall global emissions of methyl halides and how they compare to coastal ocean emissions within a similar region.

2. BACKGROUND

2.1 Methyl Chloride

CH_3Cl is the highest concentration chlorine containing compound in the atmosphere and has an atmospheric lifetime of 0.9 years [*Carpenter et al.*, 2014; *Hu et al.*, 2013; *Montzka et al.*, 2011]. It is responsible for over 15% of the chlorine present in the troposphere [*Butler*, 2000] and about 12% of the total stratospheric chlorine [*Tokarczyk et al.*, 2003]. Until around 1996 the largest source of CH_3Cl was believed to be the oceans, however, in more recent years field work revealed that the ocean source was over estimated and terrestrial plants are probably the largest source [*Carpenter et al.*, 2014; *Hu et al.*, 2010]. Terrestrial sources include biomass burning, salt marshes, wetlands, rice paddies, and tropical forests [*Carpenter et al.*, 2014]. Sinks of CH_3Cl include soil uptake, degradation in the ocean, and reactions with hydroxyl radicals [*Carpenter et al.*, 2014].

Focus has shifted to coastal environments, including coastal salt marshes, coastal wetlands, and coastal oceanic processes, as they are large sources of CH_3Cl [*Carpenter et al.*, 2014; *Hu et al.*, 2010; *R C Rhew et al.*, 2002]. Even with the recent increase in studies on coastal sources, there are still large gaps in coastal CH_3Cl data. The global budget remains unbalanced with only 83% of CH_3Cl sources being accounted for [*Carpenter et al.*, 2014]. The lack of information regarding coastal sources contributes to this imbalance, thus adding coastal and bay system information could narrow the gaps in the global budget [*Carpenter et al.*, 2014; *Hu et al.*, 2010; *Yokouchi et al.*, 2000].

2.2 Methyl Bromide

CH_3Br is the largest source of bromine to the stratosphere, with an atmospheric life time of 0.8 years [*Carpenter et al.*, 2014; *Hu et al.*, 2010; *Montzka et al.*, 2011]. In the stratosphere, bromine is 40 to 100 times more efficient than chlorine at depleting ozone through catalytic ozone destruction [*Wamsley et al.*, 1998]. A synergistic coupling between both the chlorine and bromine ozone destruction pathways can occur, which results in an increase of about 20% in destruction efficiencies of both bromine and chlorine [*Garcia and Solomon*, 1994].

Sources of CH_3Br to the atmosphere include oceanic production, biofuel emissions, biomass burning, wetland production, ride paddy production, salt marsh production, and fumigation [*Carpenter et al.*, 2014; *Yvon-Lewis et al.*, 2009]. Sinks include oceanic uptake, hydroxyl radical reactions, photolysis, and soil uptake [*Carpenter et al.*, 2014; *Yvon-Lewis et al.*, 2009]. In recent years, the atmospheric concentration of CH_3Br had decreased due to the phasing out of the use of CH_3Br as an agricultural and structural fumigant; however, quarantine and pre-shipment (QPS) uses are exempt from the phase-out [*Carpenter et al.*, 2014; *Yvon-Lewis et al.*, 2009]. The global budget for CH_3Br is unbalanced with only about 68% of the sources being accounted for (Table 1) [*Carpenter et al.*, 2014]. This imbalance is due to a lack of complete knowledge on the sources of methyl bromide. There are still many uncertainties and a lack of data on certain environments that are important in the overall budget [*Carpenter et al.*, 2014] including coastal areas such as bays, estuaries, and near shore environments.

2.3 Methyl Iodide

While CH_3Cl and CH_3Br have similar lifetimes, chemical properties, and sources, CH_3I does not. The bonds involving iodine are weak and strongly photochemically active, which leads to the quick release of iodine into the atmosphere from CH_3I [*Smythe-Wright et al.*, 2006].

Because of the weak bonds, it has a lifetime of approximately seven days, and thus little CH_3I can reach the stratosphere [*Carpenter et al.*, 2014]. CH_3I is broken down and the iodine is released primarily in the troposphere where it plays a role in the depletion of lower tropospheric ozone.

However, depletion of lower stratospheric ozone can occur even with the short lifetimes, as deep convection events can transport CH_3I from low altitudes to the stratosphere in a few hours [*Kritz et al.*, 1993; *Smythe-Wright et al.*, 2006]. Iodine containing compounds are also thought to be a component in the formation of cloud condensation nuclei (CCNs) [*Laakso et al.*, 2002]. Sources of CH_3I include biological production by rice paddies and marine environments and anthropogenic production by uses in pharmaceutical production and as a pesticide

Marine environments are the dominant source of CH_3I accounting for over 80% of the global CH_3I emissions. However, specific marine sources are not strongly constrained [*Carpenter et al.*, 2014; *Redeker et al.*, 2000; *Smythe-Wright et al.*, 2006]. Marine sources include production by macroalgae, microalgae, methylation of iodine by bacteria, and photochemical degradation of organic matter [*Brownell et al.*, 2010; *Carpenter et al.*, 2014; *Richter and Wallace*, 2004]. Research focusing on coastal production of CH_3I is limited, and it is suggested that there is a strong marine source that is missing [*Carpenter et al.*, 2014; *Smythe-Wright et al.*, 2006].

2.4 Coastal Sources and Sinks

Coastal sources, oceanic and terrestrial, of methyl halides are important in the total global budgets of methyl halides. Emissions vary both spatially and temporally in different coastal environments, such as salt marshes, estuarine systems, and terrestrial systems. Methyl halide

production along oceanic coastal regions and in large bays has been sparsely studied leading to the large uncertainties in the coastal sources and sinks.

Of previous studies that have investigated methyl halides in coastal waters *Hu et al* [2010] and *Tokarcyzk et al* [2003] report that these environments could be a large source of CH_3Br and CH_3Cl due to production by biological sources such as phytoplankton, seaweed, and sea grass. Natural production though photochemical reactions in surface seawater has also been reported [*R M Moore*, 2008]. Emissions of methyl halides in the coastal ocean have been recorded at a rate of 1.1 – 349 nmol m^{-2} d^{-1} and 0 - 12 nmol m^{-2} d^{-1} for CH_3Cl and CH_3Br respectively, with global yearly emissions estimates of 0.5 – 3.6 Gg yr^{-1} and 19 – 98 Gg yr^{-1} for CH_3Cl and CH_3Br respectively [*Hu et al.*, 2010]. Other coastal sources include wetlands, salt marshes, and coastal area rice paddies [*Drewer et al.*, 2006; *Redeker et al.*, 2000; *R C Rhew et al.*, 2002]. Emissions from wetlands have been recorded at a rate of 57.4 – 1,1109.1 nmol m^{-2} d^{-1} and 2.2 - 56 nmol m^{-2} d^{-1} for CH_3Cl and CH_3Br respectively [*Varner et al.*, 1999]. Global emissions estimates are as high as 48 Gg yr^{-1} and 4.6 Gg yr^{-1} for CH_3Cl and CH_3 Br respectively, these emissions estimates are similar to coastal ocean as global wetland area is smaller than coastal ocean area [*Varner et al.*, 1999]. Rice paddies are significant sources of CH_3Br and CH_3I, despite low total global area the global emission estimates for CH_3Cl, CH_3Br, and CH_3I are 5.3, 3.5, and 72 Gg yr^{-1} respectively [*Redeker et al.*, 2000].

The biological production of methyl halides occurs from reactions involving the methyltransferase enzyme and its catalyzation of the S-adenosyl-L-methionine (SAM) dependent methylation of halides chloride, bromide, and iodide [*Wuosmaa and Hager*, 1990]. The reactivity depends on the nucleophilicity of the acceptor anion, with iodide being the strongest acceptor, followed by bromide and chloride [*Wuosmaa and Hager*, 1990]. Iodide is preferred to bromide

and chloride at a rate that is over two orders of magnitude larger than bromide or chloride rates, this explains how CH_3I is emitted at a rate similar to CH_3Br when the concentration of iodide is typically orders of magnitude lower [*R C Rhew et al.*, 2002; *Wuosmaa and Hager*, 1990]. CH_3Cl is emitted at highest rates as chloride is the most abundant halide in seawater and soils [*R C Rhew et al.*, 2002; *Wuosmaa and Hager*, 1990]. The methyltransferase enzyme has been found to be present in microalgae, macroalgae, rice species, wetlands plant species, salt march species, and a variety of fungus species [*Carpenter et al.*, 2014; *Redeker et al.*, 2000; *R Rhew and Mazéas*, 2010; *R C Rhew et al.*, 2002; *Tokarczyk and Moore*, 1994; *Wuosmaa and Hager*, 1990]. Another natural production pathway are photochemical reactions with colored dissolved organic matter (CDOM) that can produced methyl halides [*R M Moore*, 2008; *Richter and Wallace*, 2004].

Sinks for methyl halides include both chemical and biological degradation in the ocean. Chemical degradation occurs though hydrolysis of the methyl halide or nucleophilic substitution and thus transformation of the methyl halide [*King and Saltzman*, 1997; *Tokarczyk et al.*, 2003]. Biological degradation and dehalogenation occurs by methyl halide degrading bacteria that are diverse and present in both marine and terrestrial environments. Degradation has been shown to occur in diverse environments and to be important in understanding the concentrations of methyl halides present [*King and Saltzman*, 1997; *McDonald et al.*, 2002; *Tokarczyk et al.*, 2003]. Filtration experiments show degradation is significantly faster in unfiltered samples, indicating that biological degradation can be tied to particulate matter in the water [*King and Saltzman*, 1997; *McDonald et al.*, 2002].

To better understand the global budget, increased research on coastal and bay areas is required. The goal of this project was to address the gap of knowledge regarding emissions of

methyl halides from bays by completing a seasonal study of methyl halide concentrations in Galveston Bay, TX and the West Texas Shelf. During the one year long sampling period Hurricane Harvey occurred, the scope of the study was then changed to allow for the analysis of methyl halides in Galveston Bay pre- and post-hurricane conditions.

2.5 Hurricane Harvey

On August 25th, 2017, Hurricane Harvey made landfall at Rockport, TX. Over the following days, Hurricane Harvey broke records, including rain totals over 122cm in some of Texas. Three of Houston Hobby Airport's top 5 wettest days since 1930 occurred during this time. This instantaneous influx of freshwater caused rivers levels and flowrates to reach record highs, and massive flooding to occur throughout Texas and neighboring states. The high magnitude of precipitation caused an elevated rate of freshwater being introduced to both Galveston Bay, TX and onto the West Texas Shelf. It is estimated that approximately 46 billion cubic meters of freshwater was introduced to the Gulf of Mexico from Hurricane Harvey creating a freshwater plume along the West Texas Shelf. Much of the flood waters may have come in contact with or contain untreated waste and contain pollutants from the various industries and Environmental Protection Agency (EPA) Superfund sites that exist in Houston. Flood water carrying pollutants and freshwater from precipitation can greatly alter the chemistry and biology of the areas to which it is introduced to, affecting the coastal and estuarine environments.

3. OBJECTIVES AND HYPOTHESES

3.1 Objectives

The primary objective was to examine the spatial and temporal variations in concentrations of methyl halides in the water and overlying atmosphere of Galveston Bay, TX and the West Texas Shelf. Using the water and atmospheric concentrations the emission of methyl halides from the water to the atmosphere can be calculated. Due to Hurricane Harvey, the objective was adjusted to determine the effects Hurricane Harvey on the methyl halide concentrations of Galveston Bay, TX. This study considers many factors when looking at the emission of methyl halides, including both biological and anthropogenic sources. The main factors that should affect methyl halide concentrations in Galveston Bay are the distance from the Trinity River, San Jacinto River, and the mouth of the bay, the amount of freshwater inflow, and seasonal changes in biological activity.

3.2 Hypotheses

1. Galveston Bay will be supersaturated in the methyl halides during the entire 1 year sampling period and act as a source of methyl halides to the atmosphere.
2. Concentrations of methyl halides will increase with distance from the mouth of Trinity River.
3. Immediately following the hurricane, concentrations of methyl halides in Galveston Bay will be significantly lower due to the precipitation driven freshwater flushing.
4. The West Texas Shelf will be supersaturated in the methyl halides compounds during the sampling period and act as a source of methyl halides to the atmosphere.

Information regarding methyl halides emissions in coastal environments led to the formation of these hypotheses. Past research shows that coastal terrestrial and coastal ocean regions are sources of methyl halides to the atmosphere, this information led to hypothesizing that both Galveston Bay and the West Texas Shelf will be supersaturated and sources of methyl halides. Concentrations will increase with distance from the Trinity River is hypothesized due to the major effect the freshwater flow from the Trinity River will have on methyl halide concentrations in the area. This will affect the concentrations by diluting the methyl halide concentrations with freshwater that has low concentrations of methyl halides. It will also lower both the biological and photochemical production in the region and increase degradation because of the increased turbidity and particulate matter in the water. Lower methyl halide concentrations immediately following Hurricane Harvey is hypothesized due to the amount of precipitation and freshwater introduced to the bay. This will affect methyl halides concentrations for multiple reasons: The precipitation will be aerated and in equilibrium with the atmosphere concentrations. The freshwater flow will flush the present methyl halides out of the bay and the normal biological community, lowering the concentrations and decreasing production within the bay water.

4. ANALYTICAL METHODS

Water samples were collected using a manual 5L Niskin Water Sampler. Immediately following collection with the Niskin, samples for halocarbon analysis were collected from the Niskin using 100mL gas-tight ground glass syringes. The samples were then transferred into the purge-and-trap sample storage module by injecting through a 0.2μm Media-Kap filter to remove any remaining microorganisms or suspended sediment particles. The sample storage module is a refrigerator containing 70mL glass bulbs, all connected to a 16-position loop selection valve (Valco Instrument Co.) by PEEK tubing. Sample bulbs with the tubing attached have been calibrated to determine the actual volume of sample inside each bulb and tubing. This module allows the samples to be stored in a cold, dark, gas-tight environment until they are brought back to lab to be analyzed.

The analysis was done as soon as possible after returning from the trips. The time ranged from within 24 hours to within 6 days. Each sample bulb was separately flushed into a glass sparger using ultrapure nitrogen gas and then purged at 144mL min^{-1} at 40°C. The gasses purged from the sample were then dried by flowing through a section of magnesium perchlorate. Following the drying, the analytes were preconcentrated on the first of two cyrotraps and then focused on the second cyrotrap. Both traps were held at temperatures from -70°C to -80°C and desorbed at 230°C. Once desorbed, the analytes were transferred into the Gas Chromatography-Mass Spectrometer (GC-MS) [*Yvon-Lewis et al.*, 2004]. Blanks were run after every third sample to monitor the system. Calibration gas standards were analyzed after every fourth sample to calibrate the system. Calibration standards were whole air standards calibrated against whole air standards that were calibrated against standards from National Oceanic and Atmospheric

Administration (NOAA) Earth System Research Laboratory Global Monitoring Division. Tests for purge efficiency were run by restriping a sample of seawater five times, the percentage of the total concentration in the first stripping was used to determine the purge efficiency. The percentage of total concentration for the first stripping was 99.7% for CH_3Cl, 100.0% for CH_3Br, and 75.1% for CH_3I. Reported concentrations are corrected for purge efficiencies. Tests for reproducibility were done by injecting ten samples of a single batch of pre-filtered seawater into the sample storage module and then analyzing the samples. The analytical uncertainty was 4.34% for CH_3Cl, 2.90% for CH_3Br, and 4.57% for CH_3I. Tests for sample storage stability were done by injecting fifteen samples of a single batch of pre-filtered seawater into the storage module and running sets of four samples at time periods 0 days, 3 days, and 8 days to check for variations. Tests found that variations of each compound were within the analytical uncertainty, showing now degradation or production over the time of storage.

5. GALVESTON BAY

5.1 Sampling Methods

5.1.1 Galveston Bay Site Description

Galveston Bay is a large anthropogenically, active bay with an area of approximately 1,360km^2 and an average depth of two meters. It is one of the most active shipping ports in the United States [*Rayson et al.*, 2015]. Galveston Bay is composed of four sub bays: Galveston Bay, East Bay, West Bay, and Trinity Bay (Figure 1). Each sub bay has diverse geographical features and water residence times (Table 1).

Table 1: Features and Residence Times of Galveston Bay Sub Bays. Residence time is the length of time that the water resides in the bay. Modified from *Rayson et al.* [2015].

Sub Bay	Features	Residence Time (days)
Galveston Bay	San Jacinto River	0 – 20
East Bay	Oyster Reefs	34 – 45
West Bay	Texas City Industries	0 – 45
Trinity Bay	Trinity River	25 – 35

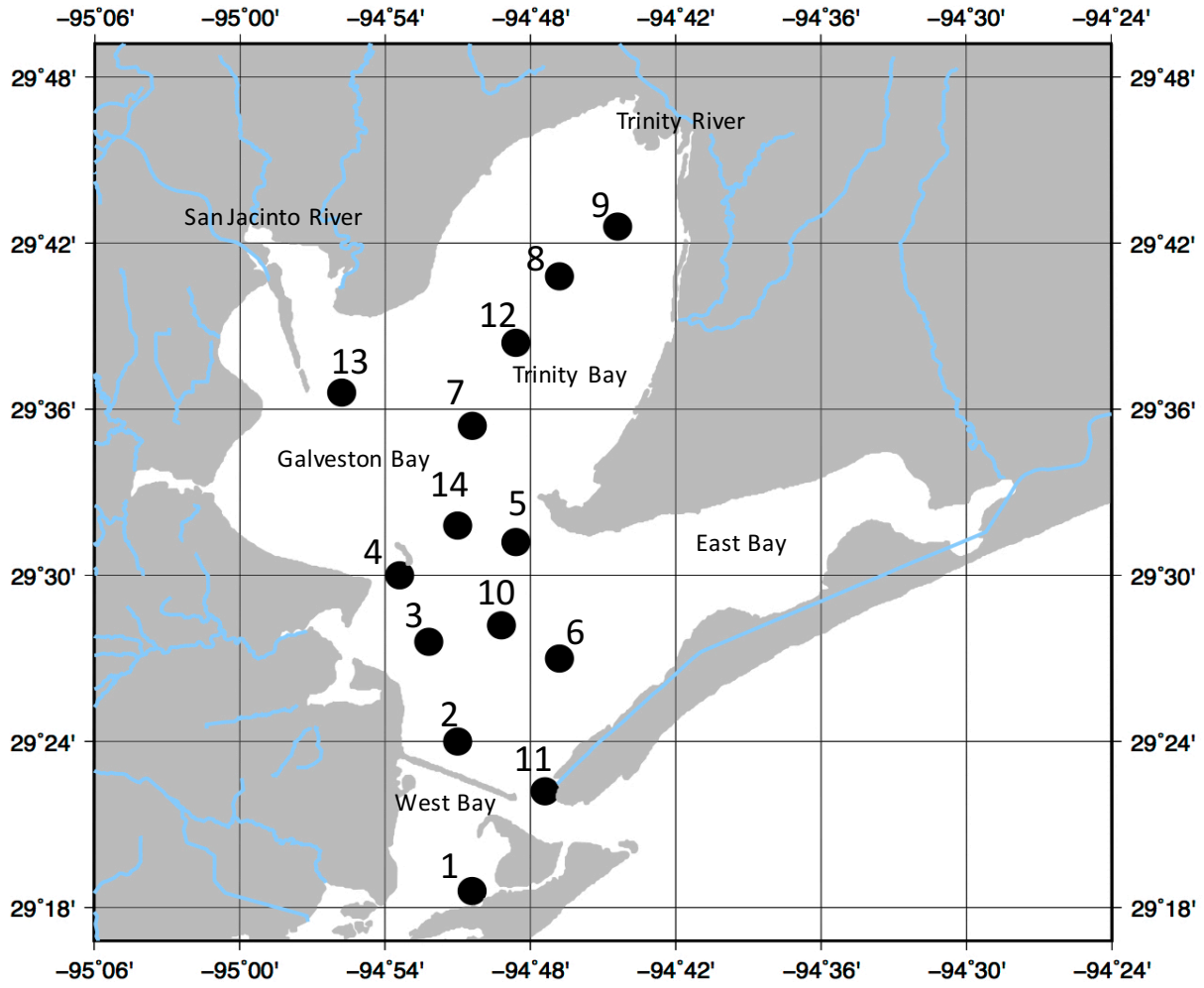

Figure 1: Sampling Map of Galveston Bay, TX. Large black dots represent sampling stations. Blue lines represent rivers flowing into Galveston Bay. Labels represent different sub bays of Galveston Bay.

The phytoplankton community in the bay has been shown to be primarily dominated by diatoms, which are known to produce methyl halides [*Lim et al.*, 2017; *Roelke et al.*, 2013]. Of known methyl halide producing phytoplankton species, five species of diatoms have been observed in Galveston Bay: *Chaetoceros sp., Navicula sp., Nitzschia sp., Odontella sp.,* and *Thalassiosira sp.* [*Lim et al.*, 2017; *Steichen et al.*, 2015]. Due to the complex environmental stressors, seasonal trends in productivity and community structure are not apparent and the

community structure changes from year to year [*Roelke et al.*, 2013]. The largest factors contributing to phytoplankton productivity are flow rates from the Trinity River and San Jacinto River. Increased Trinity flow rates lower productivity near the Trinity River mouth, while increased San Jacinto River flow rates increase phytoplankton productivity near the San Jacinto River mouth [*Roelke et al.*, 2013].

The Trinity River is responsible for about 75% of the total flow into the bay making the input from this river an important factor in controlling the chemical conditions of the bay [*Rayson et al.*, 2015]. The other inflows into the bay include freshwater inflows from the San Jacinto River, Buffalo Bayou, and seawater flowing in from the mouth of the bay. There is a large anthropogenic influence on the bay as it is located adjacent to Houston, TX, one of the most industrialized areas in the nation. Industries include shipping, refineries, water disinfection plants, and pharmaceutical production. These different industries are not a direct source of methyl halides; however, the industries could have a potential anthropogenic effect on the natural sources of methyl halides by introducing wastewater and nutrients to the bay. The diverse environments within the bay could illustrate complex interactions that lead to different concentrations and thus emission rates of methyl halides throughout the bay.

5.1.2 Galveston Bay Sample Collection

Sampling was completed at 14 stations throughout Galveston Bay (Figure 1). The stations were chosen to include the different geographical regions of the bay and to include stations near water input sources to the bay. Stations are located close to the mouth of the bay, the shipping channel, the Trinity River inflow, and the San Jacinto inflow, the distribution of stations provided a good spatial distribution of Galveston Bay and allows for characterization of the different inflow sources.

Sampling took place aboard two different research vessels: The *Lithos* and the *R/V Trident*, both Texas A&M University Galveston (TAMUG) vessels. At each sampling station, a profile of water quality parameters salinity, temperature, and density was recorded using a Castaway-CTD. A turbidity measurement was made using a Secchi disk. Water samples were collected from the surface and 1.22m above the bottom at each station. Water sampling was done using 5L Niskin Water Samplers. Water samples from the Niskin were analyzed for halocarbons. Other researchers analyzed the water samples for dissolved oxygen, dissolved inorganic carbon (DIC), alkalinity, pH, nutrients, colored dissolved organic matter (CDOM), polycyclic aromatic halocarbons (PAHs), trace metals, and dissolved organic matter (DOC). Air samples were collected in steel flasks from a sampling inlet at a height of 5m above water surface and analyzed for halocarbons.

Sampling took place over a series of five trips to Galveston Bay. Two trips took place in June, 2017, June 5th and June 8th. Stations 1-10 were sampled on these trips with samples only collected from four feet off the bottom. Two trips took place in September, 2017, September 9th and September 16th, following Hurricane Harvey. Stations 3, 5, 7, 8, and 9 were sampled at both depths on these trips. The limited number of stations sampled was due to poor weather and mechanical problems during the first of the two trips, thus all samples in September are from the September 16th sampling trip. The next trip took place on November 4th, 2017. Stations 1, 3, 5, 9, 11, 12, 13, and 14 were sampled at both depths on this trip. The addition of stations 11-14 for this trip was to get better overall coverage of the bay. Sampling was completed in a single day compared to the previous trips which included two sampling days. The last trip took place on March 24th 2018. Stations 1, 3, 5, 9, 11, 12, 13, and 14 were sampled at both depths. Similar to the November trips all of the sampling was completed in a single day.

5.2 Results and Discussion

5.2.1 Galveston Bay Water Quality Parameters

The water quality parameters of Galveston Bay varied spatially and temporally (Figure 2). The spatial trends were consistent throughout all of the sampling trips. Overall, the salinity increases moving away from the northeast portion of the bay, where Trinity River is located, towards the mouth of the bay. This is due the Trinity River, which is introducing the majority of the freshwater to the bay while seawater water is flowing in from the mouth of the bay. The temperature in the bay was relatively homogenous during every trip.

The lower temperature in November and March can be explained by seasonality (Figure 2). Stratification occurred in the bay in both June and September, but did not occur in November or March. In June, there was salinity driven stratification at stations 7, 8, and 9, all of which are near the Trinity river inflow. In September, there was a salinity and temperature driven stratification at station 3 and salinity driven stratifications at stations 7, 8, and 9.

Overall, the bay was well oxygenated during every trip. The nutrient concentrations do not have a consistent temporal trend. The concentrations in September show the biggest difference from other months concentrations (Figure 2). In September, there were high nitrate concentrations and low ammonium, nitrite, and urea concentrations compared to other months, indicating during this month the bay's water quality parameters were different than other months.

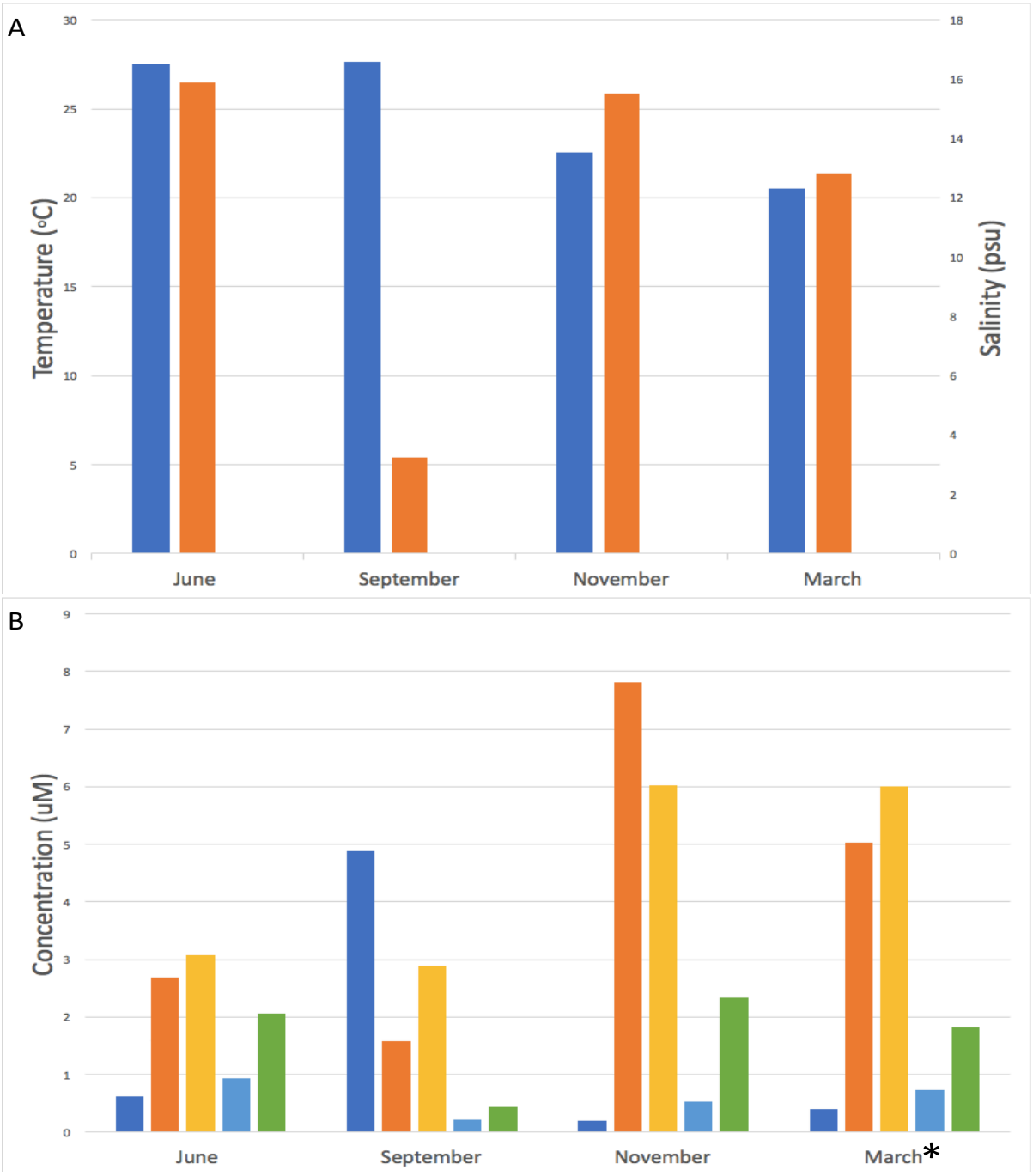

Figure 2: Bar Graphs of Average Water Quality Parameters. A. Bar graph of average water temperature (°C) (blue bar) and average water salinity (psu) (orange bar). B. Bar graph of nutrient concentrations(uM): Nitrate (blue bar), phosphate (orange bar), ammonium (yellow bar), nitrite (light blue bar), and urea (green bar). Sampling months include June 2017, September 2017, November 2017, and March 2018. The number of samples taken of nutrients for June, September, November, and March are 10, 10, 16, and 16 respectively. *Outlier removed from March nitrate data.

5.2.2 Trinity Freshwater Inflow

United States Geological Survey (USGS) water gauges were used to determine the freshwater inflow into Galveston Bay, TX. Data from three gauges were examined, (USGS 08066500) located in the Trinity River at Romayor, TX, (USGS 08074000) located in Buffalo Bayou at Houston, TX, and (USGS 08068090) located in the San Jacinto River at Porter, TX. Daily discharge data in $ft^3\ sec^{-1}$ is recorded by the gauges and was converted to $m^3\ sec^{-1}$ (Figure 3, Table 2). To determine and ensure accuracy, all the data are reviewed by USGS employees before being made available to the public.

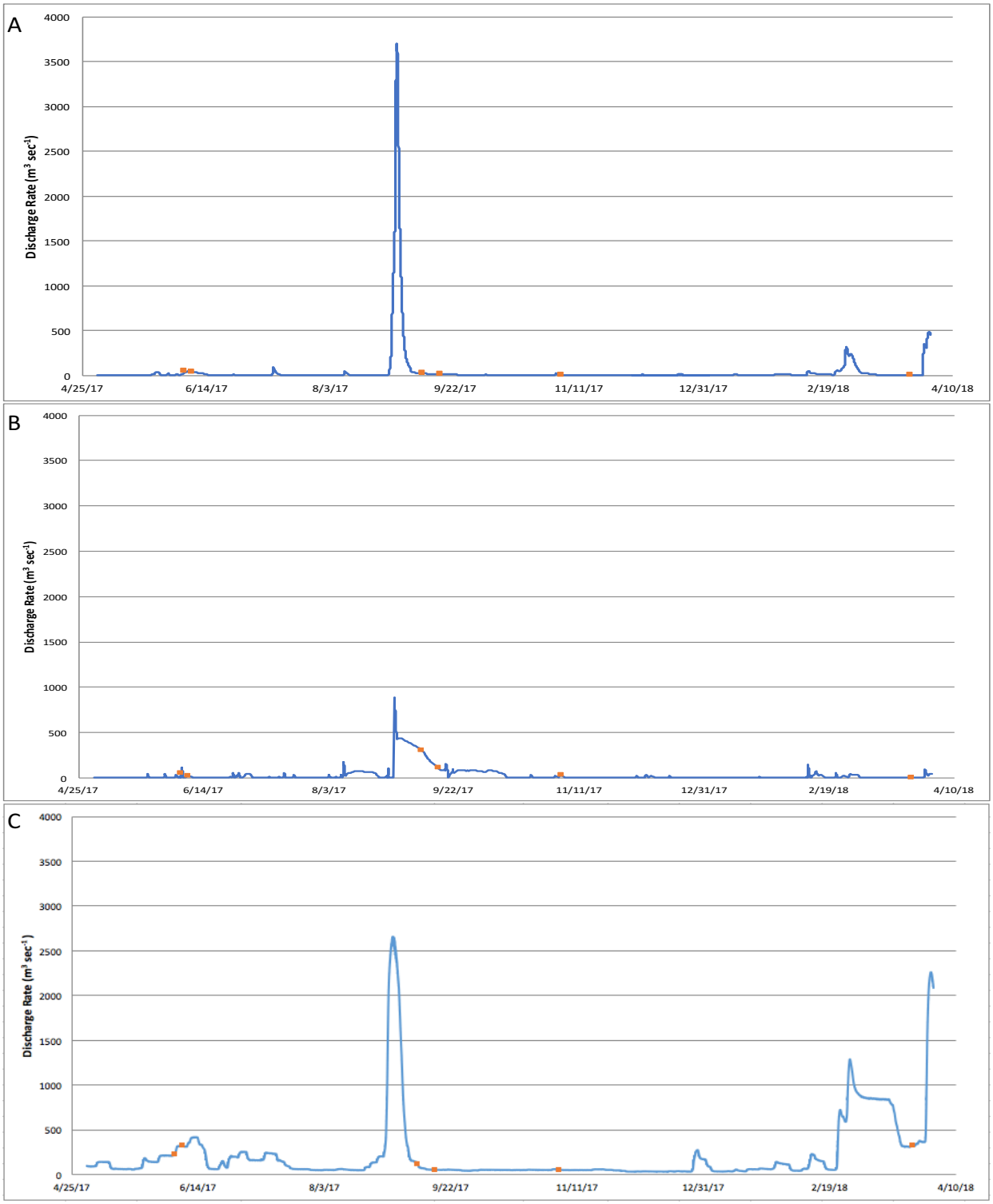

Figure 3: Discharge Rates of the Main Freshwater Sources into Galveston Bay. Orange squares represent dates that sampling took place. A. Buffalo Bayou (USGS 08074000) B. San Jacinto River (USGS 08068090) C. Trinity River (USGS 08066500)

Table 2: Average River Discharge Rate of One Month Before Sampling. Mean (min – max). Months include June 2017, September 2017, November 2017, and March 2018.The sampling period mean is the mean flow rate from May 1st, 2017 until March 31st, 2018. Data was retrieved from USGS water gauges.

	Trinity River (m^3sec^{-1})	San Jacinto River (m^3sec^{-1})	Buffalo Bayou (m^3sec^{-1})
June	141.42 (49.14 – 316.96)	12.70 (1.27 – 50.09)	4.66 (0 – 119.71)
September	550.20 (41.04 – 2657.37)	307.83 (1.13 – 2707.30)	202.76 (0 – 888.62)
November	47.15 (42.45 – 56.32)	3.57 (1.79 – 29.15)	21.98 (0 – 82.35)
March	734.30 (299.98 – 1284.82)	53.78 (3.54 – 325.45)	6.16 (0 – 40.75)
1 Year Average	208.78	39.34	29.13

The highest average discharge rates were observed in September and March. The orders of magnitude higher discharge rate in September is due Hurricane Harvey. The values recorded by the gauges may not accurately reflect this enormous freshwater influx into the bay. It would not have recorded the precipitation that was introduced directly into the bay or the floodwaters draining outside of gauged areas. Because of the large amount of precipitation and high flow rate of the water during September, the water introduced to the bay should have had a different chemical composition than normal river water, this is seen when looking at the nutrient concentrations during the month of September (Figure 2). The differences in nutrient concentrations could be due to the introduction of nutrients from overflowing waste water and sewage systems. The high volume of freshwater introduced to the bay, primarily precipitation, should also be near equilibrium with atmospheric gas concentrations as it is aerated before it reaches the bay. The high flow rates in March are due it being a wet season. Unlike September, the river gauges should accurately record the amount of freshwater introduced to the bay and that water is similar to other months chemical composition.

5.2.3 Air Mass Back Trajectories

The NOAA Air Resources Laboratory Hybrid Single Particle Lagrangian Integrated Trajectory Model (HYSPLT) was used to determine sources of the air masses present during sampling [*Stein et al., 2015*] (Figure 4). The model was run in client-server mode (HYSPLT-WEB) on the NOAA Air Resources Laboratory website. During the two sampling trips in June, the air mass came from different locations. On June 5th, the back trajectory shows that the air mass came from the middle of the Atlantic Ocean, staying over the ocean for the full 30 days leading up to sampling. On June 8th, the back trajectory came from the Atlantic Ocean, passing over the continental United States, including large areas of rice paddies (Figure 5). The air mass passes over this section of rice paddies twice in the 30 days. On September 16th, the back trajectory came from the continental United States and Canada, passing over the same region containing rice paddies as did the air mass from June 8th. On November 4th, the air mass is coming from continental Canada, passing over the western coast of Florida and looping around the Gulf of Mexico before reaching Galveston Bay. On March 24th, the air mass comes from continental United States and Canada, passing over the same region containing rice paddies as did air masses in June and September. The air mass then loops over the center of the Gulf of Mexico before reaching Galveston Bay.

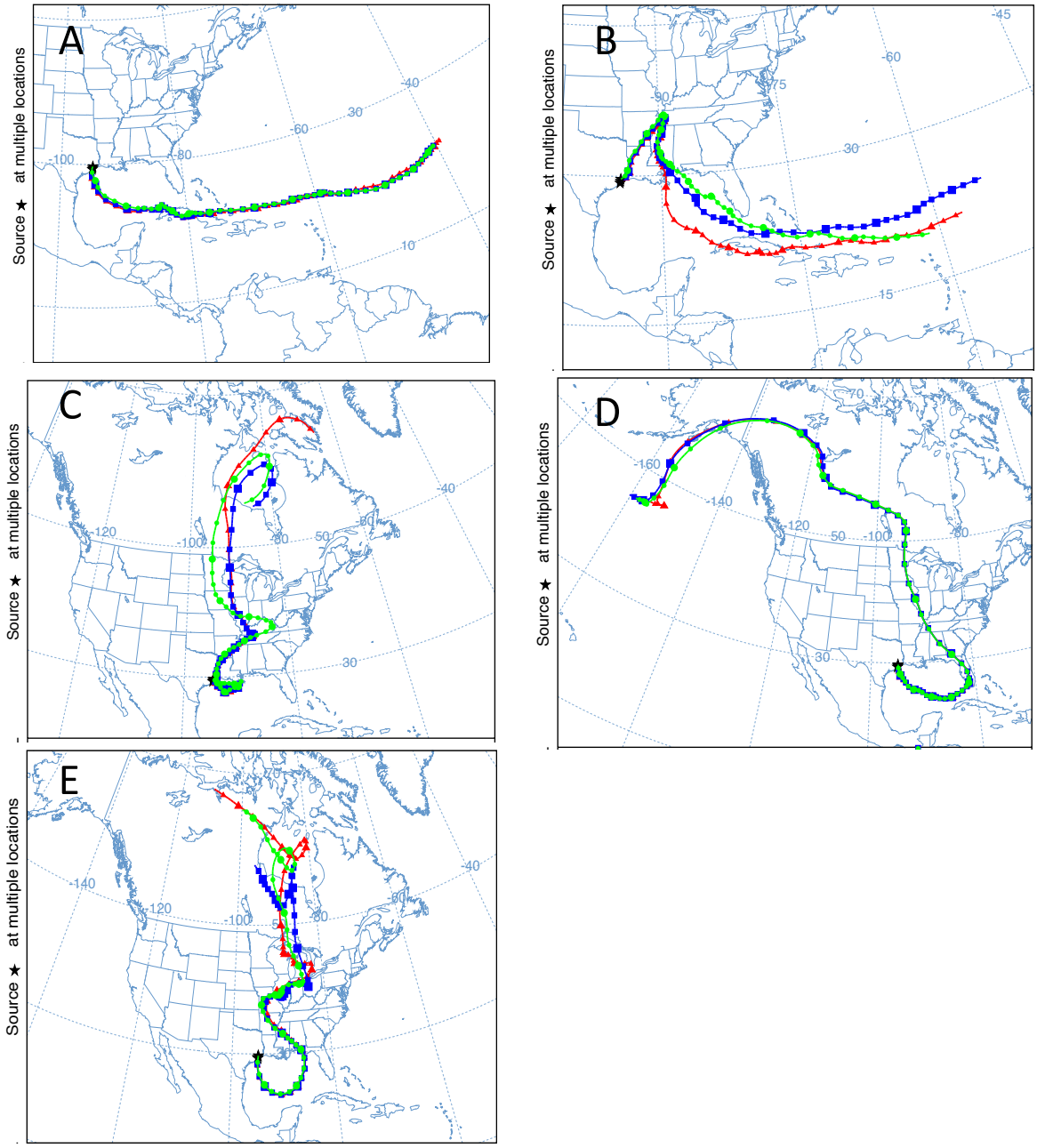

Figure 4: 30-Day Air Mass Back Trajectories. Each map shows the back trajectory of 3 sample locations at a height of 10m. Stations 1, 5, and 9 are colored green, blue, and red respectively. Each point along the back trajectory represents 6 hours. Air mass back Trajectories were created using NOAA HYSPLT model from *Stein et al.* [2015]. A. June 5th, 2017 B. June 8th, 2017 C. September 16th, 2017 D. November 4th, 2017 E. March 23rd, 2018

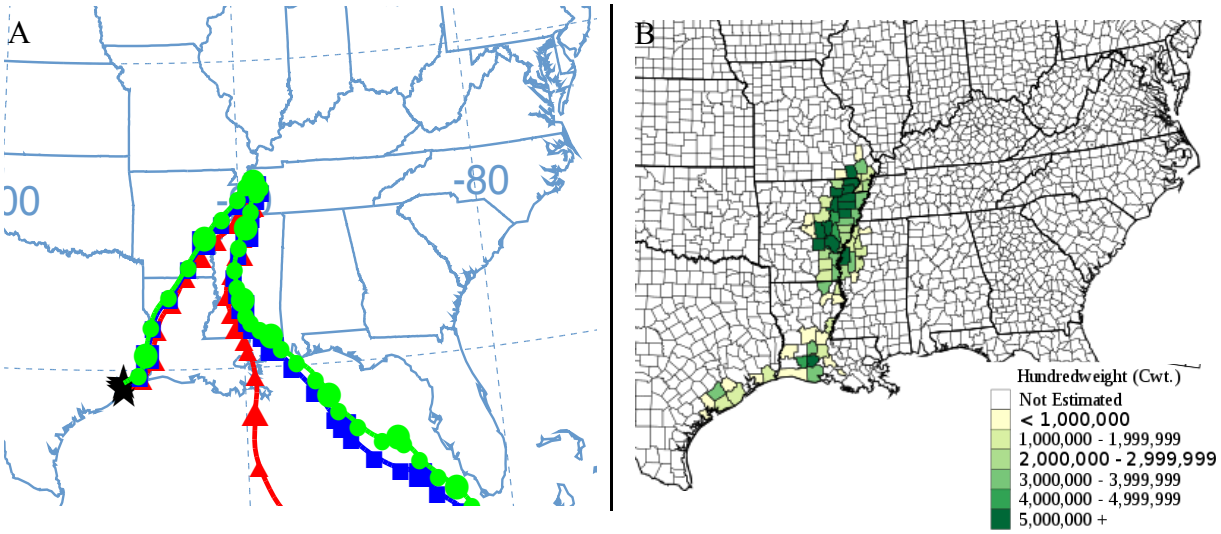

Figure 5: A. Modified Map of Rice Production in the Eastern United States (retrieved from www.nass.usda.gov). B. 30-day air mass back trajectories from June 8th at a height of 10m. Stations 1, 5, and 9 are colored green, blue, and red respectively. Each point along the back trajectory represents 6 hours. Back trajectories were created with NOAA HYSPLT model *Stein et al.* [2015].

5.2.4 Atmospheric Concentrations

The atmospheric concentrations for CH_3Br and CH_3I are show similar trends over the sampling months, with highest concentrations for both during the June sampling and lowest in March (Figure 6). High June concentrations, CH_3Br concentrations 196% above global mean, 7.0ppt, and CH_3I concentrations is 121% above the 1 year average of the Galveston Bay study, 2.81ppt, along with the trajectory data (Figure 5) suggest that the June atmospheric concentrations for both compounds are due to emission from rice paddies in the central U.S. (Figure 5). The back trajectories show that during June the air mass passed over the regions of rice paddy production twice, reaching Galveston Bay within seven day lifetime of CH_3I, during the middle of rice production season. In September, the air mass passed over a similar region but the atmospheric concentrations are not elevated, as this is after the rice has been harvested and there is no emissions of methyl halides occurring. During September, November and March, the

concentrations are slightly higher than the global mean for CH_3Br, this can be expected because of there are local sources of CH_3Br on the coast such as the coastal oceans, wetlands, and salt marshes. CH_3Cl shows a slightly different trend with 13% on average above background concentrations, 540ppt, in September, November, and March. The Atmospheric CH_3Cl concentrations in September, November, and March can be explained similarly to CH_3Br and CH_3I, elevated due to being sampled on the coast where there are local sources.

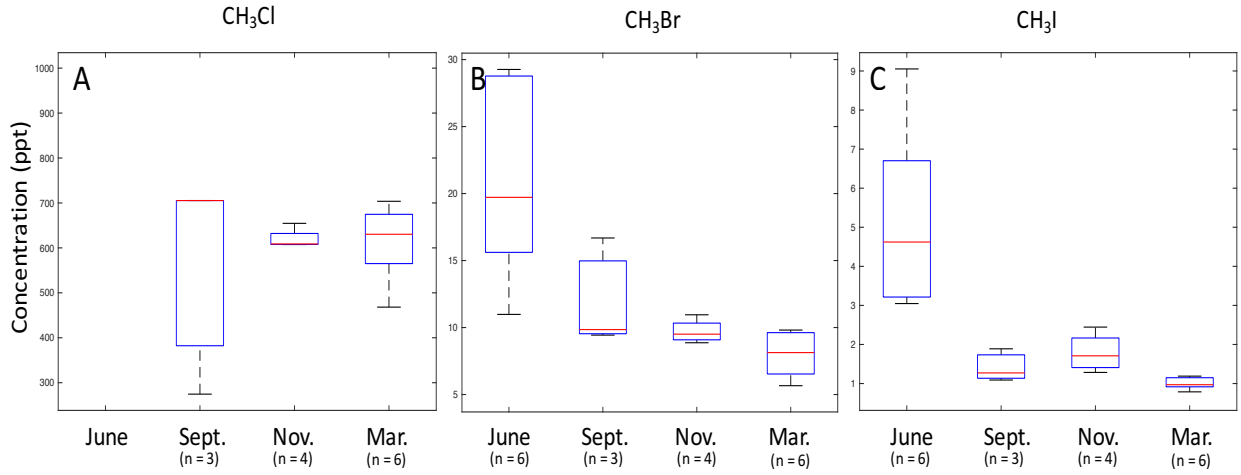

Figure 6: Boxplot of Atmospheric Concentrations. Months include June 2017, September 2017, November 2017, and March 2018. A. CH_3Cl atmospheric concentrations. B. CH_3Br atmospheric concentrations. C. CH_3I atmospheric concentrations. There are no measurements of CH_3Cl in June. There are no measurements of CH_3I in March. Parts per trillion (ppt) are units of atmospheric partial pressure. n represents the number of samples analyzed. Global mean values for CH_3Cl and CH_3Br are 540ppt and 7.0ppt respectively, global means were retrieved from *Carpenter et al.* [2014].

5.2.5 Water Concentrations

Using Spearman's rank correlation to determine relationships, the concentrations of methyl halides are spatially correlated in June and November, but not for September. In June, CH_3Br and CH_3I were correlated with a rho of 0.809 and a p value of 0.0027. In November, CH_3Br and CH_3I were correlated with a rho of 0.854 and a p value of 0.00005, CH_3Br and CH_3Cl were correlated with a rho of 0.604 and a p value of 0.017, and CH_3Cl and CH_3I were correlated with a rho of 0.579 and a p value of 0.024. In March, CH_3Cl and CH_3Br were correlated with a rho of 0.780 and a p value of 0.001. The lack of correlation between methyl halides in September is believed to be due to a disruption of the normal sources from the freshwater flush.

The spatial distribution of methyl halide concentrations at the bottom depth for each month shows a similar trend for each methyl halide (Figure 7). The spatial distribution at the surface depth also follows a similar trend as the bottom depth (Figure 8). The lowest concentrations were observed in Trinity Bay near the mouth of the Trinity River. The highest concentrations were observed in the center of the bay. November has a slightly different trend showing the highest concentrations near the mouth of the San Jacinto River for CH_3Br and CH_3I but not for CH_3Cl. The spatial trends for March again have low concentrations near the mouth of the Trinity River and high concentrations in the center of the bay; however, the trends are less apparent and CH_3Br is almost uniform throughout the bay. There were no significant correlations between methyl halides and other properties in the bay such as salinity, temperature, dissolved oxygen, macronutrients, or CDOM.

The low concentrations near Trinity River are expected for a couple of hypothesized reasons. First there is the large freshwater flow that can dilute the concentrations and lower

biological production of methyl halides in the area, the biological production is lowered near the Trinity River as the river inflow causes higher turbidity limiting the available photosynthetic radiation. This lowered biological production may lead to lower concentrations in the area. The high turbidity could also be limiting the photochemical reactions that may also lead to the production of methyl halides. Lastly, the increased turbidity in the area may allow for the enhanced degradation of methyl halides by biological dehalogenation processes tied to particles in the water [*King and Saltzman*, 1997]. Due to the limited data, it is hard to distinguish what is the main reason for the decreased concentrations in Trinity data.

The high concentrations in the center of the bay and near the mouth of the San Jacinto River suggest that there could be an increased biological source in the area. Other reasons for the elevation could be lower rates of biological production, increased photochemical production in the less turbid waters, and possible transport of methyl halides from salt marshes along the western side of Galveston Bay.

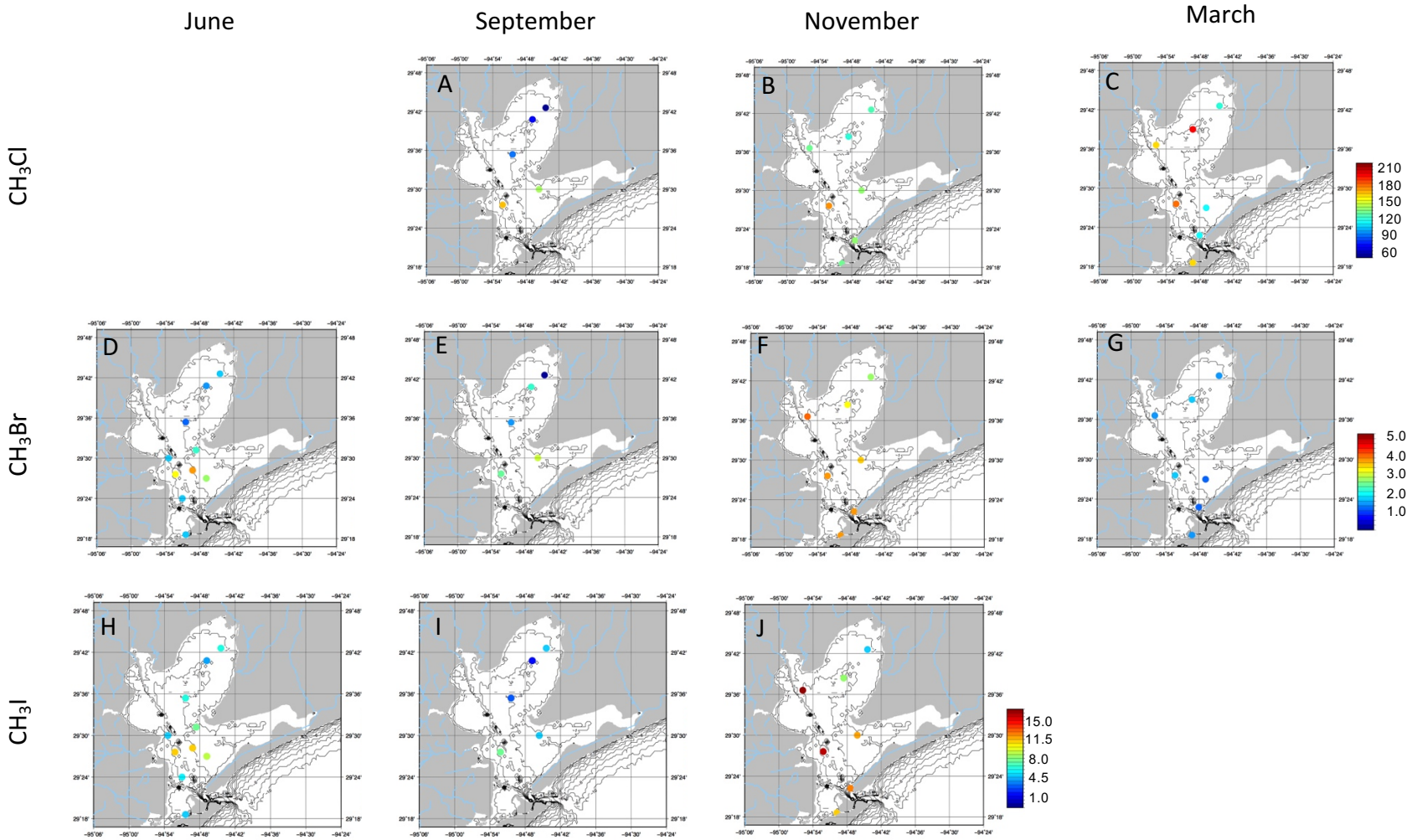

Figure 7: Maps of Methyl Halide Bottom Depth Concentrations (pM). There are no data for CH_3Cl in June and CH_3I in March. A. CH_3Cl September 2017 concentrations B. CH_3Cl November 2017 concentrations C. CH_3Cl March 2018 concentrations D CH_3Br June 2017 concentrations E. CH_3Br September 2017 concentrations F. CH_3Br November 2017 concentrations G. CH_3Br March 2018 concentrations H. CH_3I June 2017 concentrations I. CH_3I September 2017 concentrations J. CH_3I November 2017 concentrations

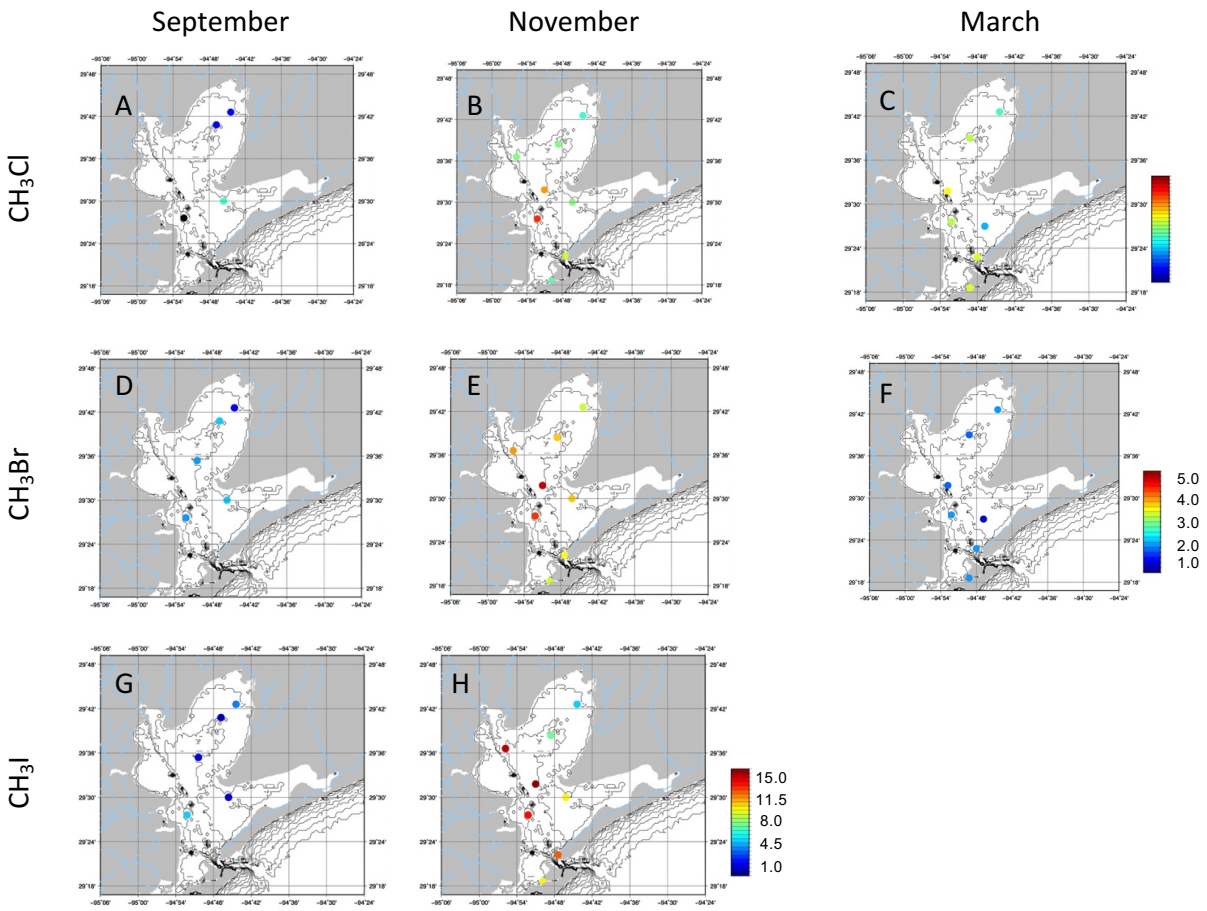

Figure 8: Maps of Methyl Halide Surface Concentrations (pM). There are no data for CH_3I in March. A. CH_3Cl September 2017 concentrations B. CH_3Cl November 2017 concentrations C. CH_3Cl March 2018 concentrations D. CH_3Br September 2017 concentrations E. CH_3Br November 2017 concentrations F. CH_3Br March 2018 concentrations G. CH_3I September 2017 concentrations H. CH_3I November 2017 concentrations.

The concentrations of CH_3Br and CH_3Cl are comparable to previous summer coastal Gulf of Mexico concentrations with CH_3Cl ranging from 61.5pM to 179pM and CH_3Br ranging from 0.8pM to 5.0pM along the coast [*Hu et al.*, 2010]. Each compound shows a similar trend of being depleted in September and elevated in November (Figure 9). March is different as it shows a different ratio between CH_3Cl and CH_3Br. CH_3Cl concentrations are high and similar to

November concentrations while CH_3Br concentrations are low and similar to September concentrations

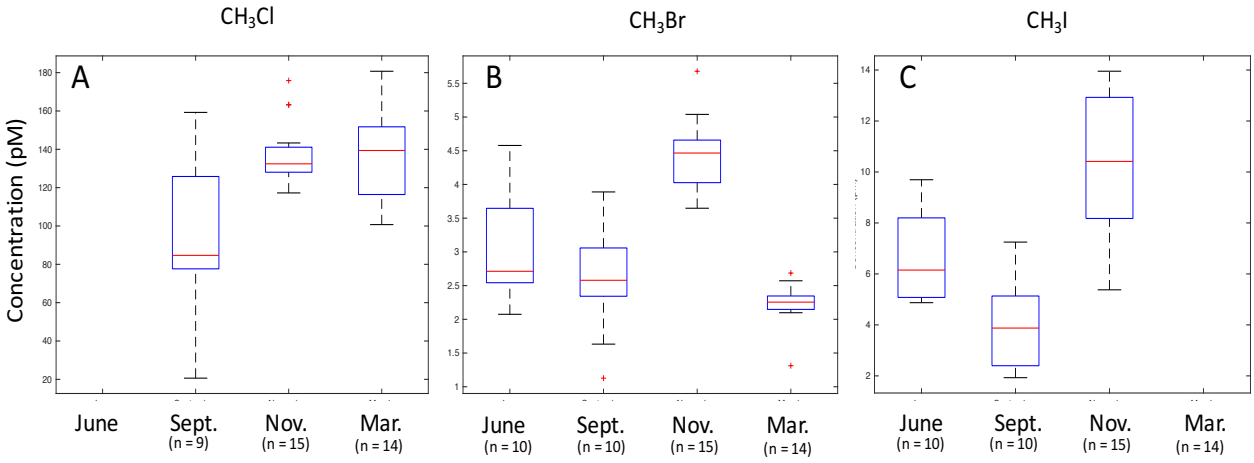

Figure 9: Boxplot of Water Concentrations (pM). Months include June 2017, September 2017, November 2017, and March 2018. There are no data for CH_3Cl in June and CH_3I in March. n represents the number of samples analyzed. A. CH_3Cl water concentrations. B. CH_3Br water concentrations. C. CH_3I water concentrations.

The lower concentrations observed in September could to be due to a freshwater flushing of the bay from Hurricane Harvey. The precipitation that was introduced to the bay would likely have had low methyl halide concentrations and been in equilibrium with atmospheric concentrations due to aeration. This flush would have also transported the methyl halides in the water and the microalgae community to outside the bay and changed the community structure within the bay [*Steichen et al.*, 2018]. During September, the community of microalgae was observed to be freshwater cyanobacteria and green algae genera. By the end of September, the estuarine and marine diatom and dinoflagellate communities appeared to have returned [*Steichen et al.*, 2018]. This could have directly affected the production of methyl halides within the water

as cyanobacteria are not known to produce methyl halides, thus the water would have stayed close to equilibrium with the atmosphere.

The high concentrations in November could be caused by the lower rate freshwater flow into the bay and a large biological rebound with a return to the normal marine community structure. The lower flow rate increases residence time in the bay and allows for methyl halides produced in the bay to reside in the water longer before being flushed out. The high inflow of nutrients, specifically NO_3^-, in September combined with the increased salinity by November could have led to a biological rebound in the normal oceanic diatom community by November causing an elevation of the emissions in the bay [*Steichen et al.*, 2018].

In March, a high concentration of CH_3Cl was observed and a low concentration of CH_3Br. The low concentration of CH_3Br was expected with the high freshwater flow rate coming in from the Trinity River, which we would expect to dilute the methyl halide concentrations and lower the biological production [*Roelke et al.*, 2013]. The high concentration of CH_3Cl is not expected due to the previously stated observations.

5.2.6 Saturation Anomalies and Sea-to-Air Fluxes

Saturation anomalies are calculated using the following equation:

$$Saturation\ Anomaly\ (\%) = \left(\frac{p_{gas,water} - p_{gas,air}}{p_{gas,air}}\right) X\ 100 \qquad (1).$$

$$p_{gas,water} = [g]_{water}/K_{H,gas} \qquad (2).$$

Where $p_{gas,water}$ and $p_{gas,air}$ are the partial pressure (atm) in the surface waters and the atmosphere, and temperature dependent $K_{H,gas}$ is the solubility of the gas (L atm mol^{-1}). The solubilities for

CH_3Cl and CH_3I were calculated using an their solubility equations [*R Moore*, 2000] and a salt out coefficient was applied [*Gossett*, 1987].

The temperature and salinity dependent solubility for CH_3Br was calculated using its solubility equation [*De Bruyn and Saltzman*, 1997]. For example, at 25°C and 35psu the $K_{H,gas}$ for CH_3Cl, CH_3Br, and CH_3I are 11.03, 7.23, and 7.41 L atm mol^{-1} respectively. If the salinity was changed to 15psu, closer to salinities observed in Galveston bay the $K_{H,gas}$ for CH_3Cl, CH_3Br, and CH_3I would decrease to 9.48, 6.33, and 6.37 L atm mol^{-1}. This indicates that the gases are more soluble in water at lower salinities. If the temperature were increased, holding salinity constant, to 29°C the $K_{H,gas}$ for CH_3Cl, CH_3Br, and CH_3I would increase to 12.76, 7.95, and 9.10 L atm mol^{-1} respectively. This indicates that the gases are less soluble at higher water temperatures. If either the water concentration is increased or the solubility of the gas in the water is decreased, holding the other constant, the saturation anomaly will increase.

The saturation anomalies show whether the water is either supersaturated or undersaturated relative to the atmosphere for each methyl halide. Positive saturation anomalies that are above zero indicate that the water is super saturated and thus a source of methyl halides to the atmosphere. Negative saturation anomalies indicate that the bay is undersaturated and thus the atmosphere is a source of methyl halides to the bay. If the saturation anomaly is zero than the water is in equilibrium with the atmosphere. To calculate the overall average saturation anomaly of the bay for a given methyl halide, the average temperature, average salinity, average surface water concentration, and average air concentration were used.

The overall sea-to-air flux of methyl halides from the bay to the atmosphere was calculated using the equation below:

$$Flux = K_{W,g}[C_{gas,water} - p_{gas,air}K_{H,gas}] \quad (3).$$

$$K_{W,g} = 0.251(U^2)(\frac{Sc}{660})^{-0.5} \quad (4).$$

where $K_{W,g}$ is the gas exchange coefficient (m d^{-1}) [*Wanninkhof*, 2014], U_{10} the 10 meter wind speed (m s^{-1}), Sc is the Schmidt number (unitless) [*Richter and Wallace*, 2004; *Tait and Moore*, 1995; *Wanninkhof*, 2014]. Due to limited wind data and meteorological stations, the 10-meter wind speed data were retrieved from the NOAA's National Data Buoy Center (NDBC) meteorological station, Station MGPT2 Morgan's Point, TX and averaged over the time period of sampling. At a wind speed of 3m s^{-1} the $K_{W,g}$ for CH_3Cl, CH_3Br, and CH_3I would be 2.44, 2.72, 2.57m d^{-1} respectively. If the wind speed was doubled to 6m s^{-1} the $K_{W,g}$ for CH_3Cl, CH_3Br, and CH_3I would be 9.76, 10.87, 10.28m d^{-1} respectively, this more than doubled the $K_{W,g}$ values. With increased $K_{W,g}$ values the flux will increase, thus showing that wind speed can be a major driver of flux along with the water and atmospheric concertation gradient. The calculated sea-to-air flux show trends similar to the saturation anomalies (Figure 10). Using the area of the bay and the averages of sea-to-air flux, the flux of the total bay area was estimated (Table 3).

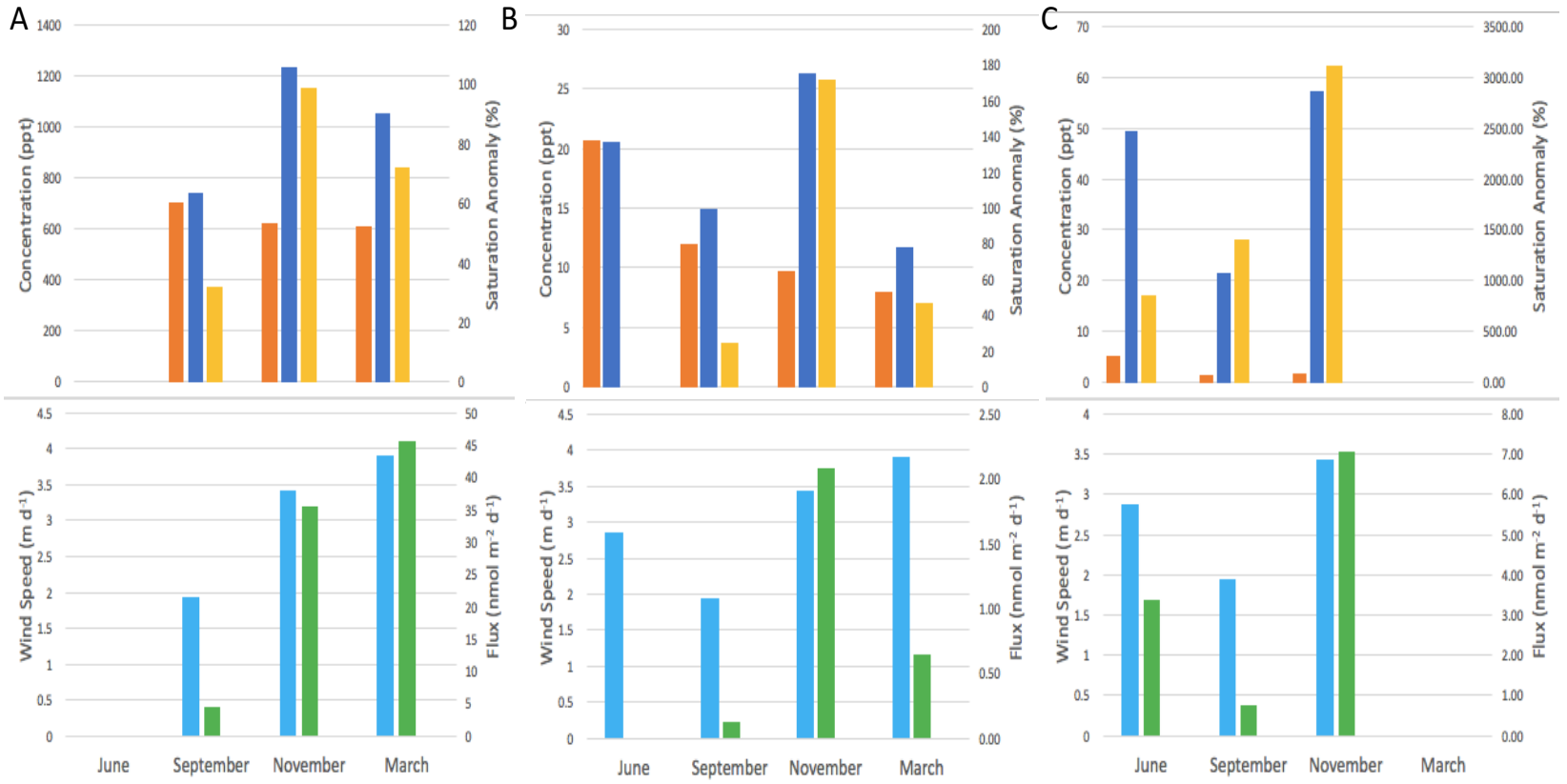

Figure 10: Bar graphs of Saturation Anomaly and Flux Parameters. Atmospheric concentration (ppt) (orange bar), water equilibrium concentration (ppt) (blue bar), saturation anomaly (%) (yellow bar), wind speed (m d^{-1}) (light blue bar), and flux (nmol m^{-2} d^{-1}) (green bar). A. CH_3Cl bar graphs B. CH_3Br bar graphs. C. CH_3I bar graphs.

Table 3: Sea-to-Air Flux of Methyl Halides Over the One Year Sampling Period. n.d. represents no data. Months include June 2017, September 2017, November 2017, and March 2018. There are no measurements of CH_3Cl in June. There are no measurements for CH_3I for March. The average sea-to-air flux for over all of the sampling months was taken to get an estimate of the 1 year average emission of methyl halides from the bay.

	CH_3Cl (Gg yr^{-1})	CH_3Br (Gg yr^{-1})	CH_3I (Gg yr^{-1})
June	n.d.	-3.55×10^{-7}	2.39×10^{-4}
September	8.62×10^{-5}	6.02×10^{-6}	5.34×10^{-5}
November	8.90×10^{-4}	9.79×10^{-5}	4.97×10^{-4}
March	1.15×10^{-3}	3.07×10^{-5}	n.d.
1 Year Average	7.10×10^{-4}	3.36×10^{-5}	2.63×10^{-4}

Overall, the CH_3Cl saturation anomaly in September is the lowest, suggesting close equilibrium with atmospheric concentrations (Figure 10). In November and March, the saturation anomalies are positive and similar throughout the bay indicating CH_3Cl production in the bay. Overall, positive saturation anomalies for all three trips suggest the bay as a source of CH_3Cl to the atmosphere. Saturation anomalies for CH_3Br and CH_3I show similar trends over the sampling trips, with low saturation anomalies in June and September and the highest saturation anomalies in November (Figure 10). The low saturation anomalies in June are due to the high atmospheric concentrations, if the atmospheric concentrations were closer to background the anomalies would have been largely positive. In September, the saturation anomalies are low, this is due to low water concentrations. In November, both compounds have their highest saturation anomalies. This is due to the high water concentrations during November. March saturation anomalies for CH_3Br are around 50%, this is higher than June and September despite the low water concentrations in March, the higher saturation anomalies are due to the lower air concentrations than in June and September (Figure 10).

The CH_3Cl sea-to-air flux during September was close to zero due to the water concentrations being close to equilibrium with the atmosphere (Figure 10). The September total sea-to-air flux from the bay is 1 to 2 magnitudes lower than the other sampling months. During the flowing months, there is a large sea-to-air flux of CH_3Cl to the atmosphere. CH_3Br shows a minimal flux from the atmosphere to the water in the month of June, this is the only time a negative sea-to-air flux is seen during the sampling trips. This is due to the high air concentrations of CH_3Br in the local atmosphere. During September, similar to CH_3Cl, CH_3Br water concentrations are almost in equilibrium with the atmosphere (Figure 10). The following months there is a consistent sea-to-air flux of CH_3Br to the atmosphere. CH_3I was seen to have a positive sea-to-air flux to the atmosphere during every sampling trip, the lowest sea-to-air flux was during September as it was closer to equilibrium with the atmosphere similar to CH_3Cl and CH_3Br (Figure 10). The total sea-to-air flux from the bay in September was an order of magnitude lower than the other months (Table 3).

6. THE WEST TEXAS SHELF

6.1 Sampling Methods

6.1.1 West Texas Shelf Site Description

The coastal area known as the West Texas Shelf in the Gulf of Mexico ranges from Port Arthur, TX to South Padre Island. This coast is home to many large cities such as Galveston, Corpus Christi, Port Arthur, Rockport, and Port Lavaca. It is also home to many bays such as Galveston Bay, Matagorda Bay, San Antonio Bay, Copano Bay, and Corpus Christi Bay. The coast contains various environments including these large bays, wetlands, and coastal salt marshes. The seafloor of the near shore coastal area tends to be soft mud that has been washed into the gulf by rivers. The region is anthropogenically influenced by many marine industries such as fisheries, oil and gas, navigation, shipping, and recreation. The area is also important in many environmental aspects such as nutrient loading, upwelling, and coastal hypoxia. Much of the nearshore environment is influenced by inflows from local rivers.

The different environments such as coastal salt marshes, wetlands, and water flow from bays could be potential sources of methyl halides [*Baker et al*., 1999; *Groszko and Moore*, 1998; *Hu et al*., 2010; *King et al*., 2000; *Sturrock et al*., 2003]. The area could help us understand how variable coastal conditions can be in methyl halide emissions. Methyl halide emissions have only been measured once in the Gulf of Mexico and very few times in other coastal areas making it an ideal location for research [*Baker et al*., 1999; *Groszko and Moore*, 1998; *Hu et al*., 2010; *King et al*., 2000; *Sturrock et al*., 2003].

6.1.2 West Texas Shelf Sample Collection

Sampling was completed at 8 stations along the West Texas Shelf (Figure 11). The cruise went from the mouth of Galveston Bay to Port Aransas along the 10m isobath. The stations were chosen to attempt to follow the freshwater plume created by the massive rainfall from Hurricane Harvey entering the coast from Galveston Bay and to analyze its coastal impacts. Sampling took place upon the *R/V Point Sur* from September 29th to October 1st. At each sampling location a profile of water quality parameters including salinity, temperature, density, CDOM, Chl a, and dissolved oxygen was recorded using a SeaBird CTD, WetLabs CDOM Fluorimeter, WetLabs Fluorimeter, and a Rinko Oxygen Sensor. Water samples from 5 depths were collected using a rosette of 12L Niskin Water Samplers and the surface and bottom samples were analyzed for halocarbons. Samples were only collected at surface and bottom due to limitations in sample storage during the trip. Other researchers analyzed discrete water samples for nutrients, DIC, alkalinity, pH, and trace metals. Air samples were collected from the bow of the vessel at six of the sample stations.

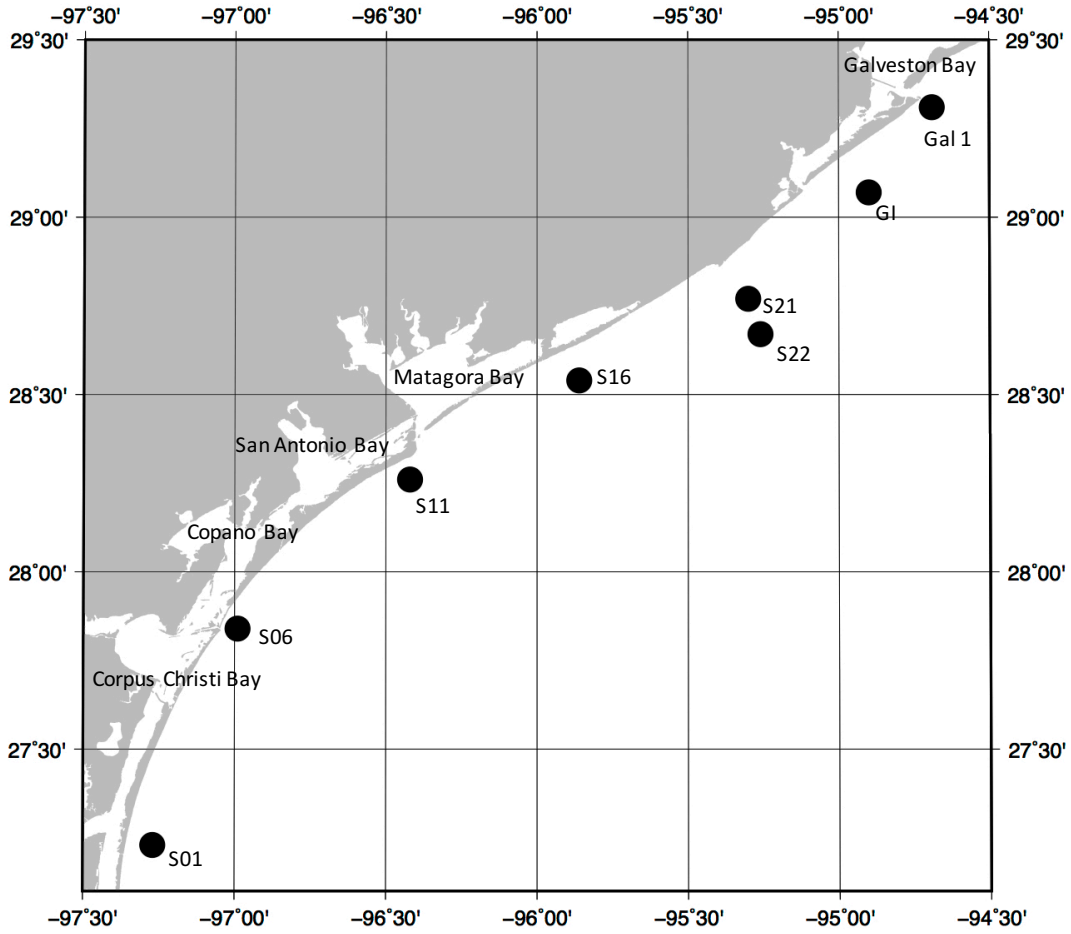

Figure 11: Sampling Map of West Texas Shelf. Large black dots indicate sampling stations. Labels show bays located on the West Texas Shelf.

6.2 Results and Discussion

6.2.1 West Texas Shelf Water Quality Parameters

The water quality parameters of West Texas Shelf varied spatially. The salinity of the West Texas Shelf averaged 27.2psu with a range of 21.0psu to 33.3psu. The lower salinities were from stations near Galveston Bay as they were still being affected by the large amount of

freshwater input during Hurricane Harvey. The temperature averaged 28.7°C with a range of 27.8°C to 29.6°C.

6.2.2 Air Mass Back Trajectories

During the first day of the sampling trip the back trajectories show that the air mass came from the south eastern United States, with some of the air mass hugging the coast of the Gulf of Mexico (Figure 12). The second day of sampling the air mass came from the continental United States. The air mass passes over areas of rice production but this sampling trip took place after rice harvesting, during times that production is not taking place. Due to no rice production, there should be no methyl halide emissions coming from rice paddies during the time of sampling.

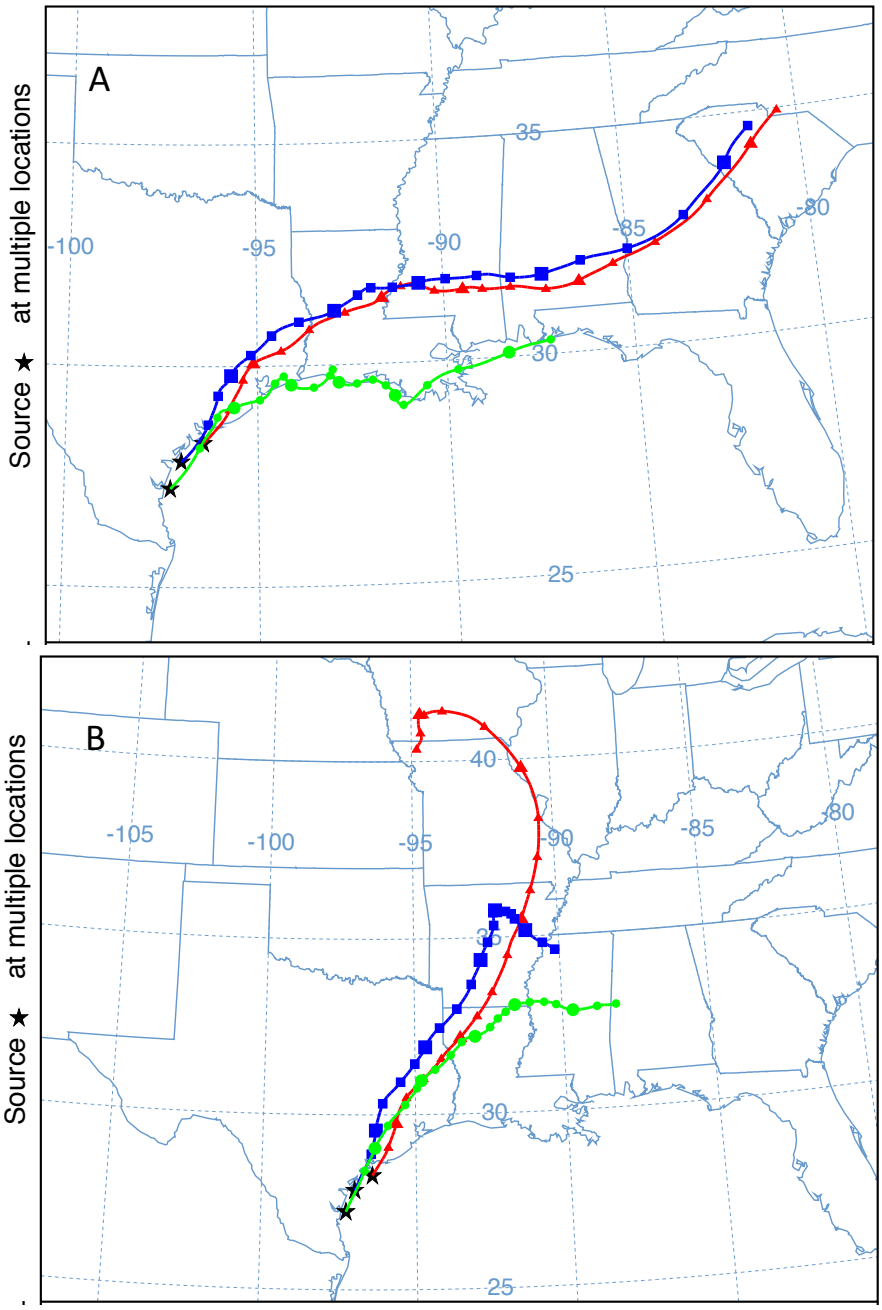

Figure 12: 5-Day Air Mass Back Trajectories. Each map shows the back trajectory of 3 sample locations at a height of 10m. Stations S01, S11, and Gal 1 are colored green, blue, and red respectively. Each point along the back trajectory represents 6 hours. Air mass back Trajectories were created using NOAA HYSPLT model *Stein et al.* [2015]. A. September 29th B. September 30th

6.2.3 Methyl Halide Concentrations, Saturation Anomalies, and Sea-to-Air Fluxes

The average and ranges of methyl halide atmospheric concentrations, water concentrations, saturation anomalies, and sea-to-air flux along the West Texas Shelf are different for each of the methyl halides (Table 4). The average atmospheric CH_3Cl concentration was 56% higher than the global mean and the average atmospheric CH_3Br concentration was 93% higher than the global mean. Saturation anomalies were calculated using equations 1 and 2 and sea-to-air fluxes were calculated using equations 3 and 4. Ten meter wind speed data was retrieved from the closest NOAA NDBC meteorological station to the location of sampling. Station GNJT2, Galveston Bay Entrance (North Jetty), TX was used for sampling locations gal1 and GI. Station FCGT2, Freeport, TX was used for sampling location s21. Station SGNT2, Sargent, TX was used for sampling location s16. Station MBET2, Matagorda Bay Entrance Channel, TX was used for sampling location s11. Station RTAT2, Port Aransas, TX was used for sampling location s06. Station BABT2, Baffin Bay, TX was used for sampling location s01. To calculate the estimated 1 year average sea-to-air flux, the area of 5,154km^2 was used as that accounts for the flux from shore to 15km off the coast and the 353km traveled along the coast during sampling. To calculate the estimated global coastal sea-to-air flux, the area of 27.123 x 10^6 km^2 was used [*Menard and Smith*, 1966]. The sea-to-air flux and estimated 1 year sea-to-air flux show that this coastal ocean can be a large source of methyl halides to the atmosphere. If the coastal emissions of CH_3Cl and CH_3Br were included in the total oceanic emissions the global emissions could be elevated by 12.5% and 4.2% for CH_3Cl and CH_3Br respectively.

Table 4: Observed West Texas Shelf Methyl Halide Parameters. Mean (min – max). Atmospheric concentrations (ppt) with 6 samples taken, water concentrations (pM) with 15 samples taken, saturation anomalies (%), sea-to-air flux (nmol m^{-2} d^{-1}), estimated 1 year average sea-to-air flux (Gg yr^{-1}) along the West Texas Shelf and estimated global coastal ocean sea-to-air flux (Gg yr^{-1}).

	CH_3Cl	CH_3Br	CH_3I
Atmospheric Concentrations (ppt)	843.8 (726 – 933.2)	13.5 (11.1 – 18.4)	1.88 (1.35 – 2.71)
Water Concentrations (pM)	140.7 (114.2 – 197.4)	2.48 (1.49 – 4.22)	5.63 (3.28 – 7.41)
Saturation Anomalies (%)	88.8	47.2	2086.4
Flux (nmol m^{-2} d^{-1})	174.87	2.64	13.45
Estimated Yearly Average Flux (Gg yr^{-1})	1.68×10^{-2}	2.53×10^{-4}	1.29×10^{-3}
Estimated Global Coastal Ocean (Gg yr^{-1})	88.2	1.33	6.79

There are no strong correlations between the methyl halide concentrations, with atmospheric and water concentrations of the same methyl halide, or the other parameters measured on the cruise. There is no clear spatial trend in any of the methyl halides with elevated or lowered concentrations with distance from Galveston Bay (Figure 13). Because of the limited amount of sampling it is hard to make any educated statement about the distribution of methyl halide emissions and sources along the coast. It can be said that the coast is a source of methyl halides to the atmosphere; however, due to lack of correlation be atmospheric and water concentrations there could be another local source affecting the atmospheric concentrations.

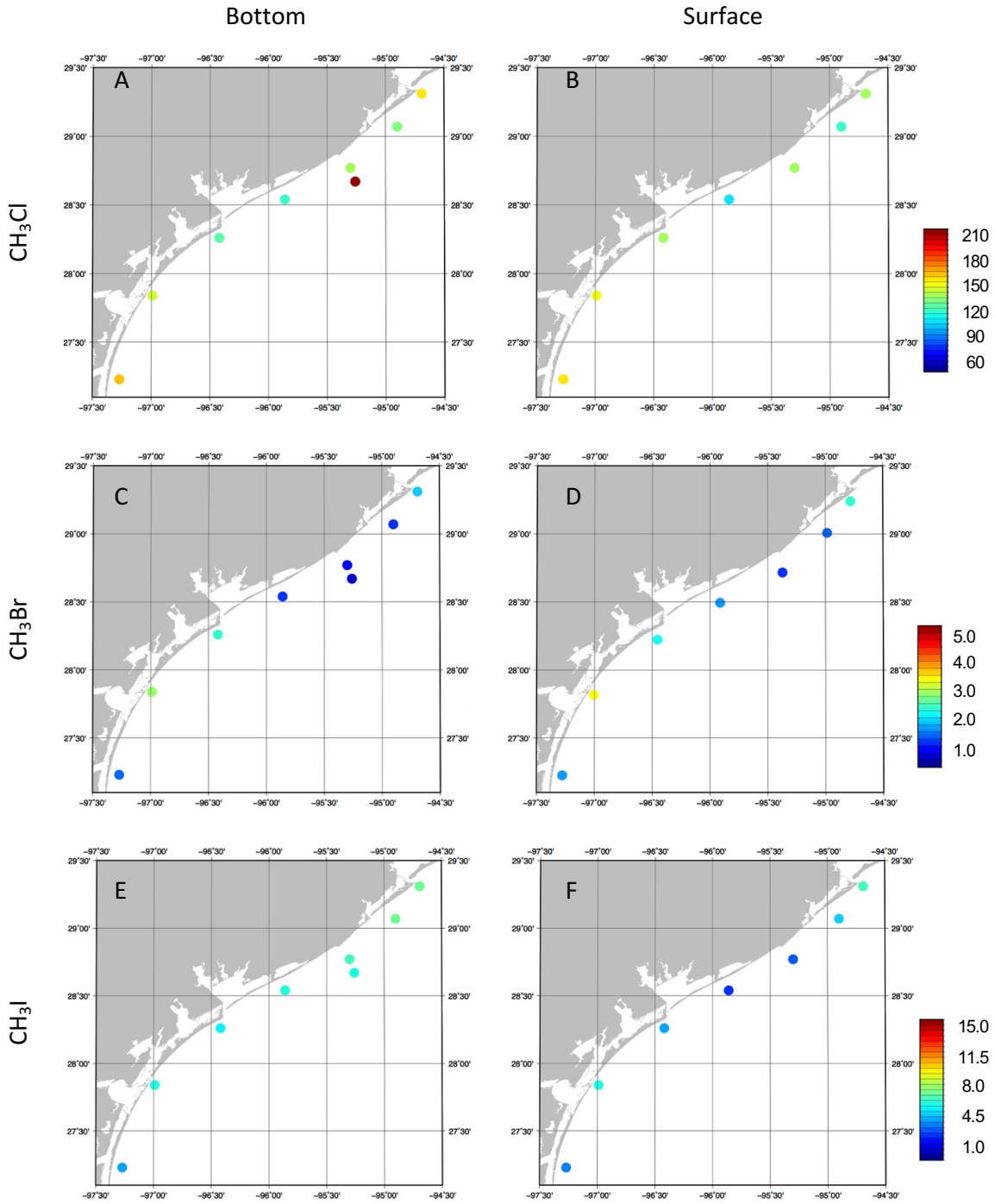

Figure 13: Maps of Methyl Halide Water Concentrations. A. CH_3Cl bottom concentrations B. CH_3Cl surface concentrations C. CH_3Br bottom concentrations D. CH_3Br surface concentrations E. CH_3I bottom concentrations F. CH_3I surface concentrations

The comparison of the coastal CH_3Cl values show the CH_3Cl water and air concentrations were much higher on average than they were when sampled in a similar area, along the Eastern United States on the GOMECC cruise in 2007 [*Hu et al.*, 2010] (Figure 14). The high atmospheric concentration may be due to a large local and coastal source of CH_3Cl to the atmosphere, with the source being much larger than during the 2007 sampling trip. The high-water concentrations suggest there is production within the water itself. The saturation anomaly was above 0% for each sample with an average of the 88.8%. The water and atmospheric concentrations are also higher than concentrations measured in the East China Sea [*Lu et al.*, 2010]. The difference between the GOMECC cruise and our cruise could show potential of seasonal variation from the CH_3Cl source, while the difference from the East China Sea could show regional variance.

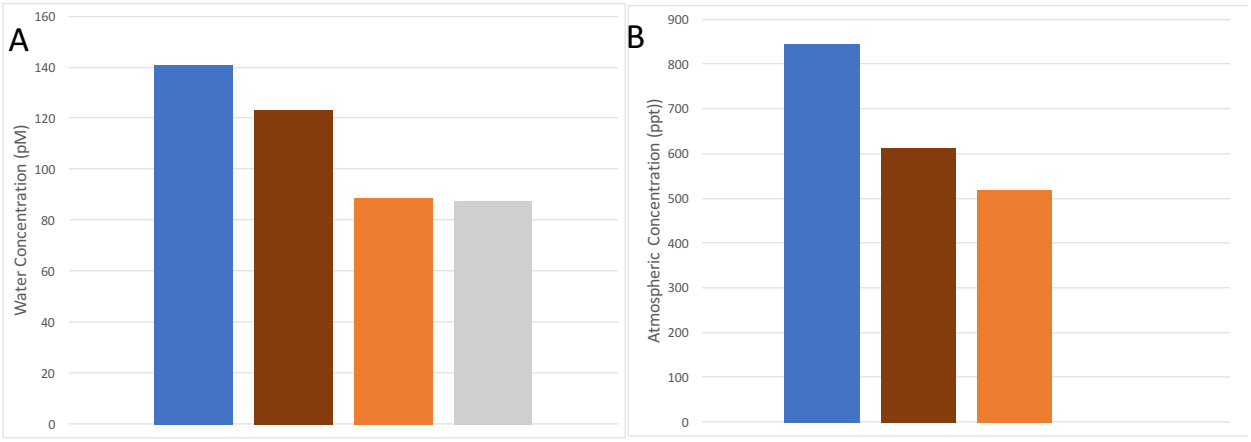

Figure 14: CH_3Cl Bar Graph of West Texas Shelf and Other Coastal Areas. Average atmospheric CH_3Cl concentrations (ppt) and water concentrations (pM). West Texas Shelf (blue bar), Galveston Bay (maroon bar), GOMECC Eastern U.S. (orange bar), East China Sea (gray bar). A. Water concentrations. B. Atmospheric Concentrations. West Texas Shelf and Galveston Bay average data from this study. GOMECC Eastern U.S. data modified from *Hu et al.* [2010]. East China Sea data modified from *Lu et al.* [2010].

CH_3Br values are slightly elevated compared to the GOMECC cruise in 2007 [*Hu et al.*, 2010] (Figure 15). however, they fall in a very similar range. This could suggest that the sources of CH_3Br during this cruise were similar to that during the GOMECC cruise with less variation than the CH_3Cl sources. The saturation anomaly was above 0% for each station with an average of 47.2%. Compared to cruises in different coastal areas, the concentrations fall within their concentration ranges [*Groszko and Moore*, 1998; *Hu et al.*, 2010; *King et al.*, 2000; *Lu et al.*, 2010], with concentrations in the North Sea and Tasmania significantly higher. The higher observed concentration were attributed to the ongoing presence or a bloom of prymnesiophytes [*Baker et al.*, 1999; *Sturrock et al.*, 2003].

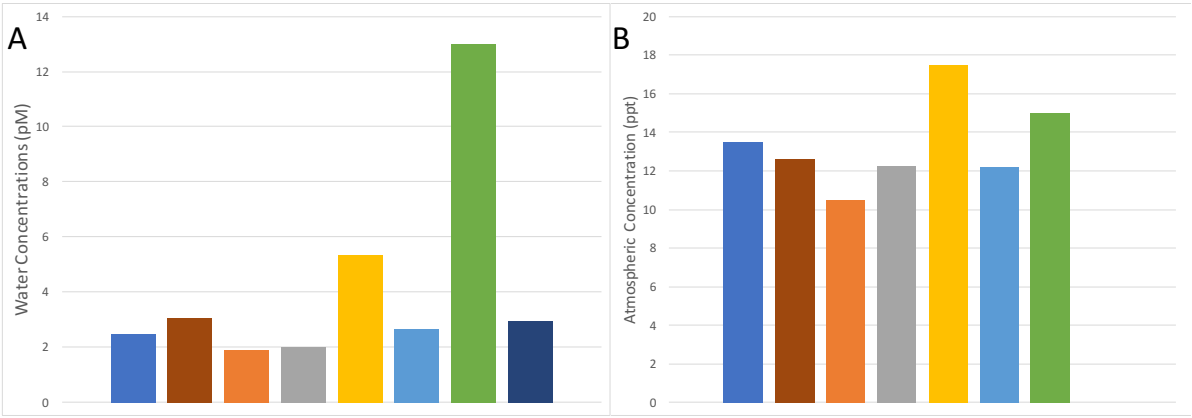

Figure 15: CH_3Br Bar Graph of West Texas Shelf and Other Coastal Areas. Average atmospheric CH_3Br concentrations (ppt) and water concentrations (pM). West Texas Shelf (blue bar), Galveston Bay (maroon bar), GOMECC Eastern U.S. (orange bar), Nova Scotia (gray bar), North Sea (yellow bar), NE Pacific (light blue bar), Tasmania (green bar), East China Sea (dark blue bar). A. Water concentrations. B. Atmospheric Concentrations. West Texas Shelf and Galveston Bay average data from this study. GOMECC data modified from *Hu et al.* [2010]. Nova Scotia data modified from *Groszko and Moore* [1998]. North Sea data modified from *Baker et al.* [1999]. NE Pacific data modified from *King et al.* [2000]. Tasmania data modified from *Sturrock et al.* [2003]. East China Sea data modified from *Lu et al.* [2010].

Sea-to-air fluxes of CH_3Cl and CH_3Br are both higher for the West Texas Shelf cruise than the 2007 GOMECC cruise [*Hu et al.*, 2010] (Table 5). This is attributed to higher overall saturation anomalies during the West Texas Shelf cruise and higher average wind speeds during sampling. Using the sea-to-air flux and total global ocean area the estimated global coastal ocean flux was calculated (Table 4). The total global coastal ocean sea-to-air flux was calculated to be 88.2Gg yr^{-1} for CH_3Cl, 1.33Gg yr^{-1} for CH_3Br, and 6.79Gg yr^{-1} for CH_3I. Compared to the estimations from the GOMECC coastal cruise the CH_3Cl estimation is 76.4% higher, but within the range of the estimations. The CH_3Br estimation is 5.0% lower, but again within the range of the estimations.

Table 5: Comparison of CH_3Cl and CH_3Br Sea-to-Air Flux (nmol m^{-2} d^{-1}). Mean (min – max). Comparison of the West Texas Shelf cruise to the GOMECC cruise. GOMECC data modified from *Hu et al* [2010].

Region	Time	CH_3Cl Flux (nmol m^{-2} d^{-1})	CH_3Br Flux (nmol m^{-2} d^{-1})	Reference
West Texas Shelf	Sept. to Oct 2017	174.87	2.64	This study
GOMECC (Coastal Latitude <30°N)	July to Aug. 2007	119 (52 – 192)	1.5 (0.9 – 2.8)	*Hu et al.* [2010]

6.2.4 Comparison to Galveston Bay, TX

CH_3Cl sea-to-air flux on the West Texas Shelf cruise was observed to be 514% higher than the Galveston Bay 1 year average, and 280% higher than the highest observed monthly average sea-to-air flux, even though the saturation anomaly is only 44% higher than the Galveston Bay 1 year average (Figure 16). This difference in the sea-to-air flux is due to average

wind speeds during the coastal cruise being higher during the coastal cruise sampling. If wind speeds were closer in magnitude to the sea-to-air flux on the coastal cruise would have been much more comparable to the Galveston Bay cruises. The average water and atmospheric concentrations of CH_3Cl are large in magnitude, suggesting a relative overall higher production along the coast than in Galveston Bay.

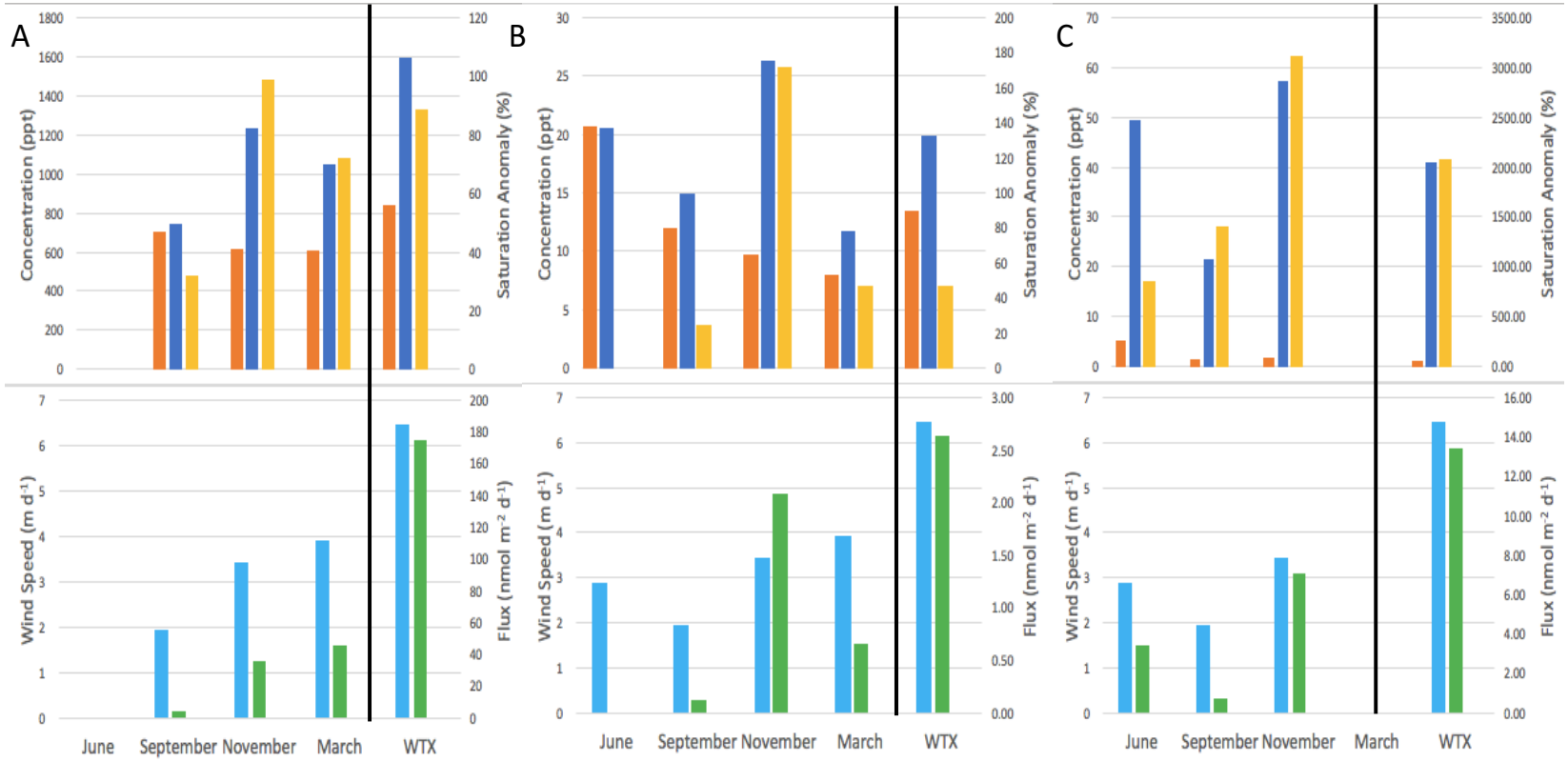

Figure 16: West Texas Shelf Comparison Bar Graphs. Atmospheric concentration (ppt) (orange bar), water equilibrium concentration (ppt) (blue bar), saturation anomaly (%) (yellow bar), wind speed (m d^{-1}) (light blue bar), and flux (nmol m^{-2} d^{-1}) (green bar). A. CH_3Cl bar graphs B. CH_3Br bar graphs. C. CH_3I bar graphs

CH_3Br sea-to-air flux along the West Texas Shelf is 231% higher than the Galveston Bay 1 year average, with it being 13% higher than the highest observed monthly average of Galveston Bay (Figure 16). The average saturation anomaly along the West Texas Shelf is observed to be lower than the average Galveston Bay saturation anomaly. The main driver of higher emissions along the West Texas Shelf is the higher average wind speeds during the coastal cruise sampling. Unlike CH_3Cl, the average water and atmospheric CH_3Br are very similar to Galveston Bay, with Galveston Bay on average having higher water concentrations. This suggests that production rate in both regions are similar, with the West Texas Shelf having higher emission rates during our sampling timeframe.

CH_3I sea-to-air flux along the West Texas Shelf is 262% higher than the Galveston Bay 1 year average, with the sea-to-air flux being 92% higher than the highest observed monthly average sea-to-air flux (Figure 16). The saturation anomaly is higher than the 1 year average anomaly of Galveston Bay, but lower than the highest monthly average saturation anomaly in November. Similar to CH_3Cl and CH_3Br, the wind speeds are the driving factor in the higher sea-to-air flux along the West Texas Shelf. Average water concentrations and atmospheric CH_3I concentrations along the coastal are lower than observed in Galveston Bay. This could indicate that there is higher production in the Galveston Bay water but less emission due to average wind speeds during our sampling timeframe.

7. CONCLUSIONS

Over Galveston Bay, the atmospheric concentrations of methyl halides suggest that during seasons of rice production, emissions from rice paddies can be a large regional source to the atmosphere. During seasons that rice is not being produced, the region of Galveston Bay has atmospheric values only slightly above background which can be expected in a coastal region due to local sources. Water concentrations of methyl halides show a precipitation driven freshwater flushing of Galveston Bay in September with near equilibrium water and air concentrations from all three methyl halides. The strong rebound in November water concentrations suggests a return to normal oceanic biological community after the flooding event in September and high production rates within the bay. This is possibly due to large amounts of nutrients entering the bay from the September flooding, allowing for elevated marine microbiological activity once the salinity levels returned to relatively normal states. March had lower concentrations of CH_3Br compared to other months, but a high concentration of CH_3Cl similar to November. The concentrations of CH_3Br and CH_3Cl were correlated suggesting they have a similar source but are being produced at a different ratio than previous months.

The spatial distribution shows that the lowest concentrations in Trinity Bay are due to various effects the inflow of freshwater from the Trinity River chemical and biological methyl halide processes. These effects include possible dilution, transport to the center of the bay, lower biological activity, lower photochemical reactions, and increased degradation of methyl halides from increased turbidity. The highest concentrations of methyl halides were observed in the center of the bay and near the inflow of the San Jacinto River, this suggests biological activity in those areas could be a main source of methyl halides in the bay; however, there could be other

factors such as increased photochemical production and transport from western Galveston Bay salt marshes as well.

Saturation anomalies for CH_3Cl were positive for the September, November, and March. The sea-to-air flux indicated that the bay was emitting CH_3Cl to the atmosphere during every season, the low sea-to-air flux rate in September indicates that the hurricane caused the bay water concentrations to be almost in equilibrium with the atmosphere. CH_3Br saturation anomalies show that the bay was near equilibrium with the atmosphere in June and September, but supersaturated in November and March. The CH_3Br sea-to-air flux shows that in June the atmosphere is a source to the bay, this is due to the high local air concentrations from rice paddy production. In September, the sea-to-air flux is similar to CH_3Cl because of the hurricane. November and March the bay is a source to the atmosphere with positive sea-to-air fluxes. More research is needed to understand what the normal state for concentrations and sea-to-air flux of CH_3Br in Galveston Bay. CH_3I saturation anomalies and sea-to-air fluxes are positive throughout every trip indicating that the bay is consistently a source of CH_3I to the atmosphere. Similar to both CH_3Br and CH_3Cl, the September sea-to-air flux is the low due to being closer to equilibrium with the atmosphere than other months.

During the West Texas Shelf cruise, the observed atmospheric CH_3Cl and CH_3Br concentrations suggest that there is a large local source of CH_3Cl and CH_3Br to the atmosphere. The elevated atmospheric CH_3Br concentrations suggest there is a source of CH_3Br to the atmosphere that is not the same as the CH_3Cl source. The CH_3Br concentrations are similar to the other coastal regions and the CH_3Cl concentrations are slightly elevated but also with in the range of other coastal regions. The water concentrations of all methyl halides show there is a source of the methyl halides in the coastal waters, with CH_3Cl having the strongest source. The

lack of correlation between water concentrations suggest that these sources could be different for the different methyl halides. The saturation anomalies of all methyl halides illustrate that the West Texas Shelf is a strong source of methyl halides to the atmosphere. Because of lack of spatial coverage and trends it is hard to determine the actual sources of each methyl halides as well as spatial variation along the coast. Overall, if the coastal emissions of CH_3Cl and CH_3Br were included in the total oceanic emissions the global emissions could be elevated by 12.5% and 4.2% for CH_3Cl and CH_3Br respectively. This indicates that coastal emission of methyl halides is important on the global scale. With little previous information regarding the West Texas Shelf methyl halide concentrations and emissions it is not possible to determine whether the freshwater input from Hurricane Harvey had an influence on the coastal emissions.

When comparing Galveston Bay to the West Texas Shelf, it was seen that the shelf was observed to have higher sea-to-air fluxes for every methyl halide. The main driver of sea-to-air flux during the sampling trips appeared to be the average wind speeds, as saturation states for Galveston Bay and the West Texas Shelf were within similar ranges of each other. Overall, the similar atmospheric and water concentration between Galveston Bay and the West Texas Shelf show they are similar coastal sources of methyl halides. However, our observations show that the West Texas Shelf and Galveston Bay appear to have different drivers and sources of methyl halides production.

The information stated shows that we can accept our first hypothesis, Galveston Bay will be supersaturated in methyl halides during the entire one year sampling period and is overall a source of methyl halides to the atmosphere. Hypothesis two, concentrations of methyl halides will increase with distance from the mouth of the Trinity River, cannot be fully accepted. There is decreased concentrations near the mouth of the Trinity River, but there is not trend with

increased concentrations with an increased distance from the river. Hypothesis three, immediately following the hurricane, concentrations of methyl halides in Galveston Bay will be significantly lower due to the precipitation driven freshwater flushing, can be accepted. The bay shows a decrease in concertation of all three methyl halides after the hurricane. Hypothesis four, the West Texas Shelf will be supersaturated in the methyl halides compounds during the sampling period and act as a source of methyl halides to the atmosphere, can be accepted.

REFERENCES

Baker, J., C. Reeves, P. Nightingale, S. Penkett, S. Gibb, and A. Hatton (1999), Biological production of methyl bromide in the coastal waters of the North Sea and open ocean of the northeast Atlantic, *Marine Chemistry*, *64*(4), 267-285.

Brownell, D., R. Moore, and J. Cullen (2010), Production of methyl halides by Prochlorococcus and Synechococcus, *Global Biogeochemical Cycles*, *24*(2).

Butler, J. H. (2000), Atmospheric chemistry: Better budgets for methyl halides?, *Nature*, *403*(6767), 260-261.

Carpenter, L. J., S. Reimann, J. B. Burkholder, C. Clerbaux, B. D. Hall, R. Hossaini, J. C. Laube, S. A. Yvon-Lewis, A. Engel, and S. Montzka (2014), Update on ozone-depleting substances (ODSs) and other gases of interest to the Montreal protocol, *Scientific assessment of ozone depletion: 2014*, 1.1-1.101.

De Bruyn, W. J., and E. S. Saltzman (1997), The solubility of methyl bromide in pure water, 35%. sodium chloride and seawater, *Marine chemistry*, *56*(1-2), 51-57.

Drewer, J., M. R. Heal, K. V. Heal, and K. A. Smith (2006), Temporal and spatial variation in methyl bromide flux from a salt marsh, *Geophysical Research Letters*, *33*(16).

Garcia, R. R., and S. Solomon (1994), A new numerical model of the middle atmosphere: 2. Ozone and related species, *Journal of Geophysical Research: Atmospheres*, *99*(D6), 12937-12951.

Gossett, J. M. (1987), Measurement of Henry's law constants for C1 and C2 chlorinated hydrocarbons, *Environmental Science & Technology*, *21*(2), 202-208.

Groszko, W., and R. M. Moore (1998), Ocean-atmosphere exchange of methyl bromide: NW Atlantic and Pacific Ocean studies, *Journal of Geophysical Research: Atmospheres*, *103*(D13), 16737-16741.

Hu, L., S. A. Yvon-Lewis, J. H. Butler, J. M. Lobert, and D. B. King (2013), An improved oceanic budget for methyl chloride, *Journal of Geophysical Research: Oceans*, *118*(2), 715-725.

Hu, L., S. A. Yvon-Lewis, Y. Liu, J. E. Salisbury, and J. E. O'Hern (2010), Coastal emissions of methyl bromide and methyl chloride along the eastern Gulf of Mexico and the east coast of the United States, *Global biogeochemical cycles*, *24*(1).

King, D. B., J. H. Butler, S. A. Montzka, S. A. Yvon-Lewis, and J. W. Elkins (2000), Implications of methyl bromide supersaturations in the temperate North Atlantic Ocean, *Journal of Geophysical Research: Atmospheres*, *105*(D15), 19763-19769.

King, D. B., and E. S. Saltzman (1997), Removal of methyl bromide in coastal seawater: Chemical and biological rates, *Journal of Geophysical Research: Oceans*, *102*(C8), 18715-18721.

Kritz, M. A., S. W. Rosner, K. K. Kelly, M. Loewenstein, and K. R. Chan (1993), Radon measurements in the lower tropical stratosphere: Evidence for rapid vertical transport and dehydration of tropospheric air, *Journal of Geophysical Research: Atmospheres*, *98*(D5), 8725-8736.

Laakso, L., J. M. Mäkelä, L. Pirjola, and M. Kulmala (2002), Model studies on ion-induced nucleation in the atmosphere, *Journal of Geophysical Research: Atmospheres*, *107*(D20).

Lim, Y., S. Phang, N. A. Rahman, W. Sturges, and G. Malin (2017), Halocarbon emissions from marine phytoplankton and climate change, *International Journal of Environmental Science and Technology*, *14*(6), 1355-1370.

Lu, X.-L., G.-P. Yang, G.-S. Song, and L. Zhang (2010), Distributions and fluxes of methyl chloride and methyl bromide in the East China Sea and the Southern Yellow Sea in autumn, *Marine Chemistry*, *118*(1-2), 75-84.

McDonald, I., K. Warner, C. McAnulla, C. Woodall, R. Oremland, and J. Murrell (2002), A review of bacterial methyl halide degradation: biochemistry, genetics and molecular ecology, *Environmental microbiology*, *4*(4), 193-203.

Menard, H., and S. M. Smith (1966), Hypsometry of ocean basin provinces, *Journal of Geophysical Research*, *71*(18), 4305-4325.

Montzka, S., S. Reimann, A. Engel, K. Kruger, W. Sturges, D. Blake, M. Dorf, P. Fraser, L. Froidevaux, and K. Jucks (2011), Scientific assessment of ozone depletion: 2010, *Global Ozone Research and Monitoring Project-Report No. 51*.

Moore, R. (2000), The solubility of a suite of low molecular weight organochlorine compounds in seawater and implications for estimating the marine source of methyl chloride to the atmosphere, *Chemosphere-Global Change Science*, *2*(1), 95-99.

Moore, R. M. (2008), A photochemical source of methyl chloride in saline waters, *Environmental science & technology*, *42*(6), 1933-1937.

Rayson, M. D., E. S. Gross, and O. B. Fringer (2015), Modeling the tidal and sub-tidal hydrodynamics in a shallow, micro-tidal estuary, *Ocean Modelling*, *89*, 29-44.

Redeker, K., N.-Y. Wang, J. Low, A. McMillan, S. Tyler, and R. Cicerone (2000), Emissions of methyl halides and methane from rice paddies, *Science*, *290*(5493), 966-969.

Rhew, R., and O. Mazéas (2010), Gross production exceeds gross consumption of methyl halides in northern California salt marshes, *Geophysical Research Letters*, *37*(18).

Rhew, R. C., B. R. Miller, M. Bill, A. H. Goldstein, and R. F. Weiss (2002), Environmental and biological controls on methyl halide emissions from southern California coastal salt marshes, *Biogeochemistry*, *60*(2), 141-161.

Richter, U., and D. W. Wallace (2004), Production of methyl iodide in the tropical Atlantic Ocean, *Geophysical Research Letters*, *31*(23).

Roelke, D. L., H.-P. Li, N. J. Hayden, C. J. Miller, S. E. Davis, A. Quigg, and Y. Buyukates (2013), Co-occurring and opposing freshwater inflow effects on phytoplankton biomass, productivity and community composition of Galveston Bay, USA, *Marine Ecology Progress Series*, *477*, 61-76.

Smythe-Wright, D., S. M. Boswell, P. Breithaupt, R. D. Davidson, C. H. Dimmer, and L. B. Eiras Diaz (2006), Methyl iodide production in the ocean: Implications for climate change, *Global Biogeochemical Cycles*, *20*(3).

Steichen, J. L., A. Denby, R. Windham, R. Brinkmeyer, and A. Quigg (2015), A tale of two ports: dinoflagellate and diatom communities found in the high ship traffic region of Galveston Bay, Texas (USA), *Journal of Coastal Research*, *31*(2), 407-416.

Steichen, J. L., Windham R., Hala D., Labonte J. M., Kaiser K., Bacosa H., Bretheron L., Kamalanathan M., Setta S., Petersen L. H., Quigg A. (2018), Rapid physicochemical and biological assessment within Galveston Bay, Texas (USA) following Hurricane Harvey [AI44D-3023] presented at 2018 Ocean Sciences Meeting, Portland, OR, 12-16 Feb.

Sturrock, G., C. Reeves, G. Mills, S. Penkett, C. Parr, A. McMinn, G. Corno, N. Tindale, and P. Fraser (2003), Saturation levels of methyl bromide in the coastal waters off Tasmania, *Global biogeochemical cycles*, *17*(4).

Tait, V., and R. Moore (1995), Methyl chloride (CH3Cl) production in phytoplankton cultures, *Limnology and oceanography*, *40*(1), 189-195.

Tokarczyk, R., and R. M. Moore (1994), Production of volatile organohalogens by phytoplankton cultures, *Geophysical Research Letters*, *21*(4), 285-288.

Tokarczyk, R., E. S. Saltzman, R. M. Moore, and S. A. Yvon-Lewis (2003), Biological degradation of methyl chloride in coastal seawater, *Global biogeochemical cycles*, *17*(2).

Varner, R. K., P. M. Crill, and R. W. Talbot (1999), Wetlands: a potentially significant source of atmospheric methyl bromide and methyl chloride, *Geophysical research letters*, *26*(16), 2433-2435.

Wamsley, P., J. Elkins, D. Fahey, G. Dutton, C. Volk, R. Myers, S. Montzka, J. Butler, A. Clarke, and P. Fraser (1998), Distribution of halon-1211 in the upper troposphere and lower stratosphere and the 1994 total bromine budget, *Journal of Geophysical Research: Atmospheres*, *103*(D1), 1513-1526.

Wanninkhof, R. (2014), Relationship between wind speed and gas exchange over the ocean revisited, *Limnology and Oceanography: Methods*, *12*(6), 351-362.

Wuosmaa, A. M., and L. P. Hager (1990), Methyl chloride transferase: a carbocation route for biosynthesis of halometabolites, *Science*, *249*(4965), 160-162.

Yokouchi, Y., Y. Noijiri, L. Barrie, D. Toom-Sauntry, T. Machida, Y. Inuzuka, H. Akimoto, H.-J. Li, Y. Fujinuma, and S. Aoki (2000), A strong source of methyl chloride to the atmosphere from tropical coastal land, *Nature*, *403*(6767), 295-298.

Yvon-Lewis, S., E. Saltzman, and S. Montzka (2009), Recent trends in atmospheric methyl bromide: analysis of post-Montreal Protocol variability, *Atmospheric Chemistry and Physics*, *9*(16), 5963-5974.

Yvon-Lewis, S. A., D. B. King, R. Tokarczyk, K. D. Goodwin, E. S. Saltzman, and J. H. Butler (2004), Methyl bromide and methyl chloride in the Southern Ocean, *Journal of Geophysical Research: Oceans*, *109*(C2).

APPENDIX A

TABLES

Table A-1: Galveston Bay June 2017 sampling data. n.d. represents no data.

Station	Depth	CH_3Cl		CH_3Br		CH_3I		Temperature	Salinity	NO_3^-	HPO_4^{2-}	NH_4^+	NO_2^-	Urea
	(m)	Air (ppt)	Water (pM)	Air (ppt)	Water (pM)	Air (ppt)	Water (pM)	(°C)	(psu)	(μM)	(μM)	(μM)	(μM)	(μM)
1	Bottom	n.d.	n.d.	16.25	2.70	3.76	5.02	27.46	22.55	1.81	1.69	3.32	3.32	1.68
2	Bottom	n.d.	n.d.	n.d.	2.54	n.d.	5.61	27.15	18.95	0.90	2.37	5.48	0.72	1.87
3	Bottom	n.d.	n.d.	10.98	4.03	3.05	9.70	27.05	17.09	2.89	3.21	3.36	1.13	2.77
4	Bottom	n.d.	n.d.	n.d.	3.14	n.d.	7.47	27.12	15.17	0.21	2.85	3.52	0.73	1.91
5	Bottom	n.d.	n.d.	23.18	2.73	5.49	5.08	27.48	15.26	0.00	2.36	1.81	0.58	1.89
6	Bottom	n.d.	n.d.	n.d.	3.65	n.d.	8.20	28.96	19.38	0.07	2.04	2.25	0.49	1.63
7	Bottom	n.d.	n.d.	28.77	2.07	9.05	6.00	27.16	14.12	0.00	3.02	1.88	0.57	2.10
8	Bottom	n.d.	n.d.	29.26	2.31	6.70	4.87	27.04	10.40	0.13	3.72	4.34	0.70	2.46
9	Bottom	n.d.	n.d.	15.61	2.56	3.21	6.30	27.07	7.42	0.31	3.44	2.57	0.56	2.68
10	Bottom	n.d.	n.d.	n.d.	4.58	n.d.	9.59	28.68	18.60	0.00	2.17	2.27	0.53	1.70

Table A-2: Galveston Bay September 2017 sampling data. n.d. represents no data.

Station	Depth	CH_3Cl		CH_3Br		CH_3I		Temperature	Salinity	NO_3^-	HPO_4^{2-}	NH_4^+	NO_2^-	Urea
	(m)	Air (ppt)	Water (pM)	Air (ppt)	Water (pM)	Air (ppt)	Water (pM)	(°C)	(psu)	(μM)	(μM)	(μM)	(μM)	(μM)
3	Bottom	n.d.	159.26	n.d.	3.46	n.d.	7.25	27.25	15.12	4.79	1.71	2.40	0.49	0.66
5	Bottom	n.d.	137.95	n.d.	3.89	n.d.	5.15	28.60	2.39	4.29	1.21	2.17	0.11	0.33
7	Bottom	n.d.	96.93	n.d.	2.48	n.d.	3.62	26.60	2.53	7.40	1.97	2.51	0.66	0.47
8	Bottom	n.d.	83.81	n.d.	3.06	n.d.	2.86	26.79	1.01	4.23	1.07	2.56	0.09	0.48
9	Bottom	n.d.	67.06	n.d.	1.13	n.d.	5.13	27.02	0.19	4.49	2.36	3.02	0.10	0.45
3	Surface	705.32	20.62	16.68	2.49	n.d.	5.13	27.09	6.04	4.65	0.96	3.10	0.25	0.49
5	Surface	n.d.	121.79	n.d.	2.74	n.d.	2.40	28.82	2.35	4.28	1.54	2.65	0.12	0.39
7	Surface	274.60	n.d.	9.85	2.34	1.09	2.19	26.50	1.84	4.65	0.70	2.87	0.16	0.34
8	Surface	n.d.	84.67	n.d.	2.67	n.d.	1.93	28.22	0.65	4.13	1.29	2.36	0.09	0.33
9	Surface	705.40	81.18	9.43	1.63	1.27	4.13	29.62	0.20	5.88	3.01	5.32	0.10	0.45

Table A-3: Galveston Bay November 2017 sampling data. n.d. represents no data.

Station	Depth	CH_3Cl		CH_3Br		CH_3I		Temperature	Salinity	NO_3^-	HPO_4^{2-}	NH_4^+	NO_2^-	Urea
	(m)	Air (ppt)	Water (pM)	Air (ppt)	Water (pM)	Air (ppt)	Water (pM)	(°C)	(psu)	(μM)	(μM)	(μM)	(μM)	(μM)
1	Bottom	n.d.	127.87	n.d.	4.56	n.d.	9.61	22.45	25.29	0.00	5.68	4.18	0.48	1.59
3	Bottom	n.d.	163.19	n.d.	4.68	n.d.	13.18	22.45	18.31	0.00	6.23	3.99	0.35	1.62
5	Bottom	n.d.	132.44	n.d.	4.47	n.d.	10.41	22.76	11.77	0.27	8.84	6.27	0.63	3.03
9	Bottom	n.d.	120.85	n.d.	3.65	n.d.	5.43	23.07	9.53	0.00	9.69	5.80	0.52	2.53
11	Bottom	n.d.	132.76	n.d.	4.53	n.d.	10.72	21.96	20.23	0.00	5.20	3.27	0.42	1.37
12	Bottom	n.d.	117.25	n.d.	4.09	n.d.	7.89	22.19	11.20	0.89	9.34	5.96	0.68	2.99
13	Bottom	n.d.	128.64	n.d.	4.94	n.d.	13.51	22.82	12.46	0.00	8.12	8.71	0.54	2.39
1	Surface	609.55	128.88	9.30	3.90	2.44	9.47	22.46	25.25	1.14	6.80	4.95	0.47	2.38
3	Surface	n.d.	175.85	n.d.	5.04	n.d.	12.24	22.50	18.31	0.00	5.98	8.93	0.47	1.69
5	Surface	607.96	134.45	8.86	4.31	1.28	9.03	22.82	11.74	0.00	8.09	5.67	0.61	2.52
9	Surface	607.44	124.18	10.95	3.76	1.53	5.38	23.18	9.52	0.00	9.79	5.71	0.62	2.63
11	Surface	n.d.	143.32	n.d.	4.01	n.d.	11.22	22.02	20.08	0.00	8.01	8.08	0.56	2.46
12	Surface	n.d.	132.55	n.d.	4.26	n.d.	7.23	22.18	11.20	0.00	8.88	5.47	0.58	2.46
13	Surface	654.62	131.81	9.71	4.60	1.89	13.16	22.85	12.52	0.65	9.16	8.45	0.66	3.11
14	Surface	n.d.	163.29	n.d.	5.68	n.d.	13.95	22.30	15.48	0.00	7.45	4.87	0.53	2.26

Table A-4: Galveston Bay March 2018 sampling data. n.d. represents no data.

Station	Depth	CH_3Cl		CH_3Br		CH_3I		Temperature	Salinity	NO_3^-	HPO_4^{2-}	NH_4^+	NO_2^-	Urea
	(m)	Air (ppt)	Water (pM)	Air (ppt)	Water (pM)	Air (ppt)	Water (pM)	(°C)	(psu)	(μM)	(μM)	(μM)	(μM)	(μM)
1	Bottom	n.d.	153.93	n.d.	2.30	n.d.	n.d.	20.04	25.71	0.03	2.11	4.79	0.62	1.42
3	Bottom	n.d.	166.03	n.d.	2.57	n.d.	n.d.	20.70	17.99	0.00	5.40	5.18	0.51	1.36
5	Bottom	n.d.	111.38	n.d.	2.10	n.d.	n.d.	20.44	14.21	0.99	3.17	6.52	0.75	2.34
9	Bottom	n.d.	116.43	n.d.	2.26	n.d.	n.d.	20.27	0.26	27.61	5.63	7.44	1.11	2.58
11	Bottom	n.d.	111.38	n.d.	2.10	n.d.	n.d.	20.26	21.24	0.00	2.14	4.89	0.60	1.42
12	Bottom	n.d.	180.73	n.d.	2.69	n.d.	n.d.	20.69	2.51	2.28	3.82	10.11	0.94	2.92
13	Bottom	n.d.	151.74	n.d.	2.25	n.d.	n.d.	20.79	8.34	0.00	11.55	6.29	0.78	1.97
14	Bottom	n.d.	n.d.	n.d.	n.d.	n.d.	n.d.	20.63	14.23	0.02	10.30	5.64	0.73	1.85
1	Surface	565.06	144.58	8.64	2.27	0.92	n.d.	20.34	23.81	0.00	1.34	3.29	0.46	0.96
3	Surface	468.20	137.82	7.61	2.47	0.79	n.d.	20.69	17.97	0.00	8.02	4.97	0.59	1.46
5	Surface	616.33	100.73	5.66	1.31	1.19	n.d.	20.44	14.17	0.00	2.29	5.22	0.60	1.51
9	Surface	703.69	123.14	9.81	2.25	0.95	n.d.	20.27	0.26	32.61	6.52	7.60	1.28	2.57
11	Surface	674.70	140.96	9.62	2.35	0.99	n.d.	20.24	19.22	0.00	1.94	4.22	0.51	1.14
12	Surface	n.d.	136.58	n.d.	2.15	n.d.	n.d.	20.72	2.52	2.40	3.99	7.48	0.83	2.40
13	Surface	644.37	n.d.	6.53	n.d.	1.15	n.d.	20.79	8.34	0.00	3.26	6.12	0.79	1.78
14	Surface	n.d.	145.16	n.d.	2.18	n.d.	n.d.	20.63	14.28	0.00	8.91	6.23	0.75	1.51

Table A-5: West Texas Shelf sampling data. n.d. represents no data.

Station	Depth	CH_3Cl		CH_3Br		CH_3I		Temperature	Salinity	CDOM	Chl a
	(m)	Air (ppt)	Water (pM)	Air (ppt)	Water (pM)	Air (ppt)	Water (pM)	(°C)	(psu)	(mg m^{-3})	(mg m^{-3})
gal1	Bottom	n.d.	153.46	n.d.	2.63	n.d.	7.41	28.27	27.17	11.39	0.84
GI	Bottom	n.d.	132.21	n.d.	1.97	n.d.	7.29	27.79	30.90	5.39	0.38
s21	Bottom	n.d.	135.73	n.d.	1.67	n.d.	6.97	27.95	30.84	6.25	0.48
S16	Bottom	n.d.	120.47	n.d.	1.81	n.d.	6.04	28.51	31.19	5.87	0.54
S11	Bottom	n.d.	126.87	n.d.	3.18	n.d.	5.52	28.68	28.90	5.00	0.86
S06	Bottom	n.d.	142.53	n.d.	3.54	n.d.	6.01	28.91	25.79	8.52	0.88
S01	Bottom	n.d.	158.54	n.d.	2.13	n.d.	4.96	28.96	26.46	7.04	0.69
S22	Bottom	n.d.	197.37	n.d.	1.49	n.d.	6.34	28.38	33.31	2.74	0.64
gal1	Surface	918.02	135.14	18.41	3.20	2.71	6.86	29.62	21.02	13.76	1.79
GI	Surface	n.d.	122.14	n.d.	2.01	n.d.	5.09	29.09	25.20	8.19	1.77
s21	Surface	739.19	135.40	11.10	1.81	2.10	3.72	29.01	27.03	6.52	0.82
S16	Surface	726.43	114.16	11.52	2.26	1.77	3.28	28.88	24.35	9.92	0.51
S11	Surface	933.22	138.37	15.58	2.80	1.92	4.68	28.99	25.66	8.20	0.86
S06	Surface	915.18	146.94	11.41	4.22	1.39	6.30	28.90	24.84	8.62	1.09
S01	Surface	830.69	150.69	13.15	2.41	1.35	4.05	28.81	25.63	6.91	0.76